UNIVERSITAT DE BARCELONA

Final Degree Project

Biomedical Engineering Degree

"Dynamic PET-Tau Quantification for Progressive Supranuclear Palsy Diagnosis"

Barcelona, 22nd January 2024

Author: Santiago Romaní

Director/s: Aida Niñerola, Raúl Tudela

Tutor: Raúl Tudela

Abstract

Tauopathies are neurodegenerative diseases caused by the abnormal accumulation of tau proteins in the brain. One uncommon tauopathy is progressive supranuclear palsy (PSP), whose symptoms often overlap with other brain disorders, and its detection is only possible postmortem since there is not an available ideal biomarker.

PET-tau imaging has the potential to revolutionize the early detection of this disease. PET is a nuclear imaging test which allows seeing the functionality of organs and tissues in vivo using a radiotracer that emits radiation from inside the body. A new PET tracer called 18F-PI-2620 has shown promising results concerning the detection of PSP, with high affinity to tau aggregates and low off-target binding.

This project consists of designing and testing a software for the quantification of PET images of the brain with a dynamic acquisition, which show the radiotracer distribution through time. The software performs a coregistration of the images to the standard space, where the different regions of the brain can be segmented using an atlas, and provides two physiologically meaningful parameters which are the Distribution Volume Ratio (DVR) and Standardized Uptake Value Ratio (SUVR). It gives out the DVR and SUVR values for any region of interest, as well as parametric images which help visualizing the radiotracer distribution in the brain.

A set of brain PET images from 13 subjects acquired using 18F-PI-2620 has been used for the development and testing of the software, divided into healthy controls, subjects with Down syndrome, some of whom have developed Alzheimer's disease (AD), which also implies a higher amount of abnormal deposited tau proteins. The results have shown higher DVR and SUVR values for several brain regions in those subjects who have developed AD, confirming that they have a higher radiotracer uptake and a greater amount of deposited tau proteins. This proves the correct functionality of the software and its potential as a future tool for detecting tauopathies such as PSP in combination with the radiotracer.

Acknowledgements

I want to thank Aida Niñerola and Raúl Tudela for offering me the opportunity to work on this project, and for their unmeasurable help and guidance during its development. Also, I thank my companions of the UB Biomedical Imaging Group for the advice and aid I have gotten from them, and especially to Lluis, who has been an amazing support.

Thanks to my family, friends, and Maria, whose support is always a reason to keep working.

List of figures

List of tables

Glossary

AD	Alzheimer's disease
aDS	Asymptomatic Down Syndrome
AG	Amygdala
ATLMP	Anterior Temporal Lobe Medial Part
BP	Binding Potential
dDS	Demented Down Syndrome
DS	Down Syndrome
DVR	Distribution Volume Ratio
FG	Fusiform Gyrus
HC	Hippocampus
LG	Lingual Gyrus
MNI	Montreal National Institute
MRI	Magnetic Resonance Imaging
PC	Precuneus
PET	Positron Emission Tomography
PSP	Progressive Supranuclear Palsy
PT	Putamen
PVC	Partial Volume Correction
PVE	Partial Volume Effect
ROI	Region of Interest
SUV	Standardized Uptake Value
SUVR	Standardized Uptake Value Ratio
TAC	Time-Activity Curve
TH	Thalamus
VOI	Volume of Interest
V_T	Distribution Volume

Contents

1. Introduction

1.1 Motivation

Some neurodegenerative diseases are caused by the accumulation of misfolded proteins in the brain. These are known as prionic proteinopathies and, until a few years ago, their presence could only be confirmed through postmortem brain tissue examination. The most common cause of dementia is Alzheimer's disease (AD), making up 60% to 80% of the cases. This disorder is caused by the progressive extracellular accumulation of the beta-amyloid protein fragment and intracellular twisted strands of the tau protein [1]. The **accumulation of tau proteins** forms a heterogeneous group of neurodegenerative diseases called tauopathies, which range from AD to atypical parkinsonian syndromes like **progressive supranuclear palsy (PSP)** and various rare diseases [2]. The different isoforms of accumulated pathological misfolded tau proteins that are found in neurodegenerative diseases different from AD are summarized as non-AD tauopathies. Those can be categorized according to different groups of underlying tau isoforms into dominant three repeat (3R), dominant four repeat (4R), and mixed 3R/4R tauopathies [3].

The imaging of pathological accumulated misfolded tau gives us many potential applications for **positron emission tomography (PET)**, especially in terms of differential diagnosis between tauopathies, which often overlap with other neuropathological entities [4].

Tau-specific radiotracers for use with PET have been developed for nearly ten years. Compared to beta-amyloid, the detection of tau is complicated by the presence of different isoforms and an overall lower quantity of tau aggregates in the brain [5]. The greatest challenge for the next generation of tau radiotracers is to adapt to the varying structures of isoforms and improve off-target binding. This project focuses on the potential of new 2nd generation PET tau radiotracers as biomarkers for detecting tauopathies, specifically the rare neurodegenerative parkinsonism of PSP.

PSP is a 4-repeat tauopathy whose clinical symptoms and subtypes often overlap with other neurodegenerative diseases. Thus, clinical assessments in PSP are lacking sensitivity early in the disease course and have a limited specificity for the pathologic entity [6]. This pathology can manifest in different ways, such as Richardson's syndrome (PSP-RS), as well as its Parkinsonian variant which is often indistinguishable from Parkinson's disease (PSP-P) [7].

Currently, PSP represents a clinical challenge due to the difficulty of obtaining a definitive diagnosis in life; we can just speculate based on the presence of characteristic symptoms, and it can only be confirmed by a post-mortem study. No available biomarker currently fulfils the criteria for an ideal biomarker, which would be positive in a pre-symptomatic stage, specific for any variant of pathology, and anticipate disease progression [6].

This uncommon brain disorder causes serious problems with walking, balance, and eye movements. It worsens over time and can lead to life-threatening complications, such as pneumonia and choking. There's no available cure, so treatment focuses on managing the signs and symptoms [8].

One of the most promising aspects in the search for an early and precise in-vivo diagnosis of PSP is tau biomarkers. As mentioned before, the abnormal accumulation of tau proteins is a distinctive trait, and it is involved in the pathogenesis of this illness. Recently, a PET tracer called **18F-PI-2620** has been showing promising results in this field. This novel PET tracer adheres selectively to the tau protein, making it able to identify its quantity and distribution in the brain. It has shown high affinity to pathological tau aggregates, with no relevant off-target binding towards beta-amyloid and other molecules [9].

Molecular formula	$C_{15}H_9[^{18}F]N_4$
Molecular weight	263.266
Chemical structure	

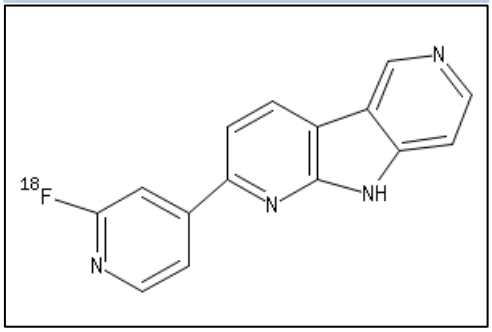

Figure 1. Chemical information about 18F-PI-2620. [74]

The incorporation of this tool in brain imaging has the potential to revolutionize the early detection of PSP and improve the quality of life of the people affected by this disease, helping them in making clinical and lifestyle decisions. This will also allow for the identification of those patients who could benefit from clinical trials where different therapeutic strategies are evaluated. Additionally, it could constitute a surrogate endpoint allowing for measuring the clearance (elimination) of this protein by the administration of certain drugs. Early and precise PSP detection would aid in distinguishing it from other brain disorders and enhance the possibility of eventually finding a treatment.

1.2 Objective

This work is part of an ongoing project from Early Stage Plus Intramural Projects from CIBER-BBN, called *Quantification tools for a novel tau PET marker in a rare neurological disease: 18F-PI-2620 in Progressive Supranuclear Palsy*, coordinated by Raúl Tudela Fernández, from CIBER-BBN, and in conjunction with CIBERNED.

My purpose in this project consists of designing and testing a methodology for the **quantification of dynamic PET images**. The principal goal is to program a software that can quantify dynamic PET images and test it using a set of images acquired with the PET-tau radiotracer 18F-PI-2620. New radiotracers usually need to be studied in dynamic PET studies (which show the radiotracer distribution through time), so the quantification methodology will focus on this type of image.

The main points to accomplish during the development of the project are the following:

- Do an exhaustive review of previous studies with 18F-PI-2620 and gather information about their approaches for the quantification.
- Investigate and evaluate different methods and existing software for PET image quantification and understand their advantages and limitations.
- Coding of a software able to perform a quantification of any dynamic PET image of the brain, able to extract physiologically meaningful parameters and generate parametric images.
- Test the software and analyse the results obtained from the quantification process using a given dataset of images acquired with 18F-PI-2620.

It is important to note that we will work with an already existing set of PET images. The project doesn't include the image acquisition and initial processing of raw PET data, such as image reconstruction.

1.3 Methodology and dataset

The development of the project takes place during the first semester of the 2023-2024 course, so the time limitations are subject to this period. Since it is about research and coding, it can be done anywhere if I have access to a computer. However, I will use the biophysics laboratory in the Hospital Clinic university faculty to be able to work alongside my tutor and colleagues of the UB Biomedical Imaging Group (BIG-UB) and to use *a local* computer there, since it operates faster than my personal laptop and can run libraries based on Linux OS. When needed, I will do a remote connection to that computer, using Filezilla and Putty, two software that allow accessing files and running code remotely. For image visualization, I will use the software ITK-Snap [10], and all the software will be coded using Python programming language.

To be able to develop and test the software, I have been given a set of images from the nuclear medicine department from *Hospital de la Santa Creu i Sant Pau* through an internal agreement. These are PET images of adults with Down syndrome (DS), acquired using the second-generation PET-tau tracer 18F-PI-2620. The dataset includes images from a total of 13 subjects. There are 7 subjects without cognitive impairment (control), 3 subjects with asymptomatic DS (aDS) and 3 demented subjects (dDS), which are patients with DS who have developed Alzheimer's.

Down syndrome is currently considered a genetic form of Alzheimer's disease. People with DS develop early-onset AD due to an extra copy of the amyloid precursor protein gene, present on chromosome 21 [11]. Subjects who have developed AD should have an increased amount of accumulated tau proteins in the brain, resulting in a higher overall radiotracer uptake, so this dataset will enable the evaluation of the software and see the validity of our quantification methodology, which is intended to be used for PSP detection in the future.

For each subject, the dataset includes a PET image with a dynamic acquisition (4D) of 6 frames and 5 minutes per frame, as well as an anatomical image from T1 weighted magnetic resonance imaging (MRI). In addition, the dataset provides a set of static (3D) PET images for each subject created by averaging the 6 frames in the dynamic image. Also, there is an excel file that classifies the different subjects into their respective types, and a JSON file for each image that describes their acquisition process. The number of frames is quite low, since this set of images is likely aimed at a static analysis. However, future clinical trials for PSP are expected to be performed in different conditions that allow the analysis of dynamic images, so our quantification methodology will be designed concerning this.

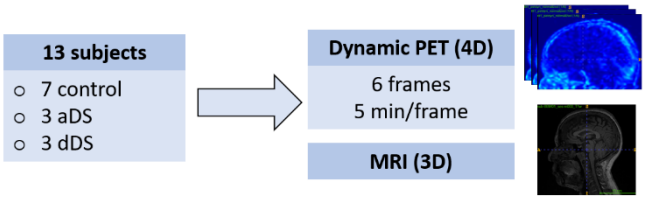

Figure 2. Diagram of the images for the development and testing of the software.

2. Background

2.1 Dynamic PET imaging

PET is a nuclear imaging test that produces images which enable visualization and measurement of a diverse range of biological processes in vivo. The test uses a safe, injectable radioactive chemical called a radiotracer and a device called a PET scanner [12]. PET allows the evaluation of the functionality of organs and tissues.

This imaging technique works by using a scanning device (Figure 3) with a big hole in its centre (where the patient is placed) that detects photons emitted from the organ or tissue that is being examined. When we unite a radioactive substance with chemical substances that are naturally utilized by an organ or tissue during its metabolic process, we obtain a radiotracer, which will travel to the targeted region and emit radiation from there. PET images can be used in conjunction with other tests, such as computed tomography (CT) or MRI. While PET informs us about the biochemical changes taking place in the body, these tests help us visualize the structure, so we can better determine where this activity is happening [13].

Figure 3. Siemens PET scanner. [75]

The radiotracer is administered through an intravenous line into the bloodstream and, as the radioisotope decays to a stable state, positrons[1] are emitted and will travel a short distance (typically <1 mm) and find an electron. The positron and electron will annihilate, giving birth to two photons in opposite directions. The scanner detects these photons, and a computer uses the information to create an image map of the studied organ or tissue. PET scans take 10-40 minutes to complete and are painless [14].

Depending on the goal of the scanning, we can use different composites. There is a library of existing radiotracers that enable the quantitative imaging of physiological, biochemical, and pharmacological targets and processes, including blood flow, metabolism, receptors, transporters, enzymes, and labeled drugs themselves, so we can often detect atypical metabolic activity in diseases before they are shown in other imaging tests. For example, in brain imaging, we can apply a radioactive atom to glucose to create a radiotracer called fluorodeoxyglucose (FDG), since the brain uses glucose for its metabolic processes. PET is used for many clinical and research applications, especially in oncology, cardiology, and neurology [15].

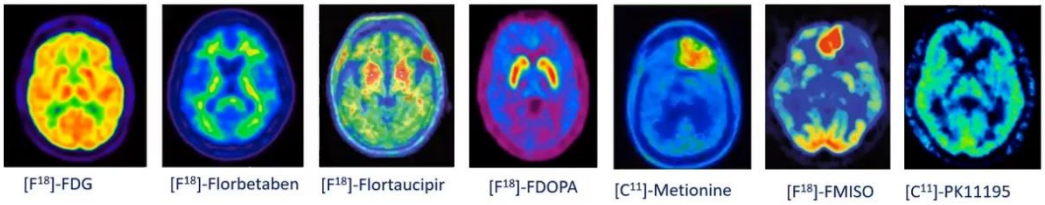

Figure 4. PET images from different radiotracers. [23]

[1] Elemental particle, the antiparticle of the electron. It has a positive charge.

PET is usually based on capturing the spatial distribution of the radiotracer with a three-dimensional scan, using static scanning (a single frame) at a time point after the injection. However, in our project we are going to focus on the quantification of dynamic images. Dynamic PET imaging, in contrast to static PET, is measured in a four-dimensional spatiotemporal distribution of the radiotracer inside our body. This involves a series of frames acquired at regular intervals following the injection of a radiotracer. The number of frames is very variable, with shorter intervals between frames providing higher temporal resolution but potentially requiring more data processing and imaging time [16].

Dynamic PET data provides a more complex set of biological parameters from the radiotracer with more specificity than the ones available from static images, being able to quantify different components of the radiotracer interaction with our body, such as the delivery of the tracer into tissue or the interaction with protein targets [17]. When a new radiotracer is introduced into the market, dynamic studies must be done before using the radiotracer for static studies. Dynamic imaging has been researched for decades and has great potential for clinical applications. Some limitations to consider are:

- Increased challenges with patient comfort and motion, due to longer scan times.
- Lack of whole-body implementations. While there have been significant efforts in single-bed dynamic PET imaging, the popularity and value of whole-body PET imaging to assess disease distribution throughout the body has implied single-frame (static) imaging [17].

2.2 PET quantification

After a PET scanner takes the images, they need to be quantified. PET quantification refers to the process of measuring and analysing the activity levels of radiotracers in PET images. It involves the use of specialized software and algorithms to calculate quantitative measurements that provide information about the metabolic activity or distribution of the radiotracer in the body. Thanks to the quantification we can obtain parametric images that describe the radiotracer uptake according to a physiological parameter.

PET quantification is important for accurate diagnosis, treatment planning, and monitoring of various diseases, including cancer, neurological disorders, and cardiovascular conditions. Factors such as imaging hardware, reconstruction software, and image acquisition protocols can influence the accuracy and reliability of PET quantification. Advances in PET technology, including new imaging hardware and reconstruction algorithms, have led to improvements in quantification accuracy and image interpretation in recent years [18].

Concentrations in PET image files are real numbers in real units. These numbers are positioned in a 3D spatial coordinate system, where each point corresponds to a small volume called voxel. Each voxel represents a defined volume and can be localized by coordinates on a three-dimensional grid [19]. For PET, these numbers are related to the radioactivity concentration (kBq/ml)[2] in a determined point of the injected radiotracer. In dynamic studies, the PET scanner measures the concentration of radioactivity for each time frame, providing quantitative 4D images.

[2] The becquerel (Bq) is the SI unit of radioactivity.

We can relate these numbers to an image by assigning a range of concentration values to a certain colour to show a colour image (Figure 5). We can select different lot of colour scales (grey, rainbow, hot metal…). Said process helps the human eye and emphasize certain structures and differences [20]. It is important to do a control over this scale to apply the same conversion between different images.

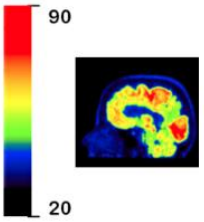

Figure 5. Colour scale. [20]

From patient preparation to image interpretation, every step of preparing the patient, acquiring, and processing PET images, and choosing criteria to quantify and interpret the data potentially affects quantitative and diagnostic accuracy [21].

2.3 Segmentation, coregistration and normalization

An important step for quantification is the separation of the different regions in the image. To extract the numbers from a defined section in a PET image, we must define a volume of interest (VOI). This process is known as image **segmentation**. When studying brain images, we want to know the radiotracer uptake in the different regions of the brain, so we must find a way to distinguish them.

A common method in brain imaging is to perform a **coregistration** to an anatomical image. Coregistration consists of the alignment between functional and anatomical images (PET-MRI, for example) of the same individual. Affine transforms, which include displacement, rotation, reflection, zooming, and shearing, are frequently employed in this process [22]. If we overlay the functional and anatomical images, we will be able to distinguish the metabolic processes happening in each region of the brain and delimit the regions of interest (ROIs).

The next usual step in brain segmentation is the **normalization** of the image. Normalization serves to align data for multiple subjects. If we want to compare the brains of different people, we must have all of them in a standard space. This is done by coregistering the anatomical and functional images into a standard template of the brain. One of the more widely used today are templates from the Montreal Neurologic Institute (MNI), which were derived from MRI scans of several hundred healthy young adults [22]. With the help of a brain atlas in the MNI space, we can easily segment different regions for any brain image in this space.

2.4 Pharmacokinetics

The values we measure in PET images are associated with the radiotracer concentration. Now, if we want to relate quantitative values (kBq/ml) to physiologically meaningful parameters, we need to apply kinetic modelling techniques, aimed at dynamic imaging.

What we are seeing in our image is not only the radiotracer binding into the sites we wanted; there are other factors we must consider. In the measured image we have four contributions, which are affected by the properties of the tissue and the radiotracer [23]:

- **Specific uptake of the radiotracer**. It is the radioligand binding to the target receptor. These are the target cells the radiotracer was designed for, and it's the one we are interested in seeing. If the radiotracer we are using is reliable, this uptake should be the highest, but PET signal is never proportional to the specific radiotracer binding.

- **Non-specific uptake of the radiotracer**. This is the result of the radiotracer binding to other sites that aren't the target.
- **Free radiotracer in the tissue**. The radiotracer isn't bound to anything, it is free in the tissue.
- **Radiotracer in blood.** In any region, there is a part of the signal that comes from blood since there are vessels in that zone.

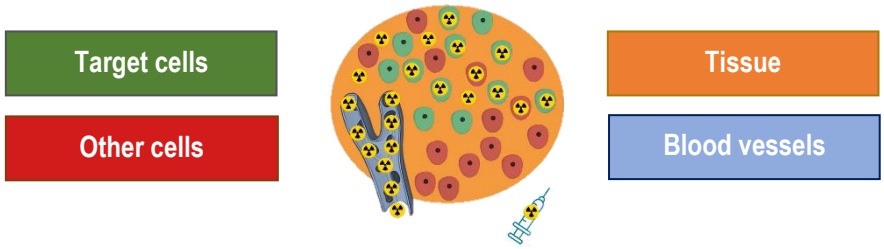

Figure 6. The different contributions to the PET signal. [23]

In PET images we are acquiring information about the radioactivity in the blood vessels present in the location we are interested in, so if we took that information into account the results wouldn't be accurate. To solve this problem, we use the **input function**. The input function or delivery function describes the concentration of the unchanged (non-metabolized) compound in arterial plasma as a function of time. This function is needed in a study to normalize the tissue concentration to the administered dose so that we can compare different studies [24].

The blood radioactivity concentration can be directly estimated from blood using the arterial plasma as input function (blood sampling), but we want to avoid this approach as much as possible since it is a challenging procedure. It is possible to do a non-invasive estimation of the blood input function, without the need for blood sampling, by using a reference region, if it exists [24]. If we take a region of interest and compare it with a reference region where there is no specific uptake of the radioligand, we can cancel out the arterial concentration.

To study the pharmacokinetics of a radiotracer, the selection of appropriate kinetic models for PET quantification is of great importance. **Compartmental analysis** is the gold standard of tracer kinetic analysis of PET and parametric imaging. In compartmental models, the physiological system of dynamic processes in the tissue of interest is decomposed into different compartments that interact with one another. These systems can be described by a system of linear differential equations and can be applied to determine parametric images [25].

Compartmental models are used in many fields, such as pharmacokinetics, epidemiology, biomedicine, engineering, etc. By assumption, inside a compartment the tracer is evenly distributed: there is no diffusion or other barrier inside the compartment [26]. They can have a physical or chemical distinction and can be reversible or irreversible. In an irreversible compartment, once something enters it can't leave, while in a reversible it can.

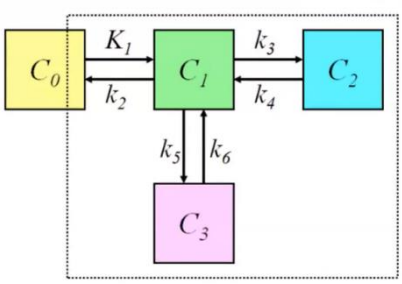

Figure 7. General kinetic compartmental model. [26]

For each compartment we add, we will be adding two extra parameters. Figure 7 shows a general kinetic model, where we consider a compartment for each concentration. $C_0(t)$ is the blood radiotracer concentration, $C_1(t)$ is the free concentration in tissue, $C_2(t)$ is the specific radiotracer concentration (binding) and $C_3(t)$ is the non-specific radiotracer concentration.

Once we define our model, we can define differential equations whose solutions will estimate the parameters. The parameters to estimate are the microparameters we see next to each arrow in Figure 7 (k_1, k_2, k_3, k_4), and macro-parameters, which are combinations of microparameters, such as the distribution volume (V_T). To do so, we do a non-linear fit to the time course of the dynamic data. If we have too many kinetic constants, we are at risk of overfitting [25]. For Figure 7, the equations are:

$$(a)\quad \frac{dC_1(t)}{dt} = K_1C_0(t) - (k_2 + k_3 + k_5)C_1(t) + k_4C_2(t) + k_6C_3(t)$$

$$(b)\quad \frac{dC_2(t)}{dt} = k_3C_1(t) + k_4C_2(t) \qquad (c)\quad \frac{dC_3(t)}{dt} = k_5C_1(t) + k_6C_3(t)$$

Equation 1 (a, b, c). Differential equations for the general kinetic compartmental model

Some of the most relevant parameters we can estimate from kinetic modelling the volume of distribution (V_T), binding potential (BP) and the unidirectional uptake rate constant (Ki). These are summarized in Table 1.

		Two-tissue approach
Volume of distribution (V_T) $V_T = \frac{C_T}{C_P}$	Represents an individual drug's propensity to either remain in the plasma or redistribute to other tissue compartments. It is the ratio of the radioligand concentration in the tissue's target region to that of the concentration of unchanged radioligand in plasma at equilibrium. [27]	$V_T = \frac{k_1}{k_2}(1 + \frac{k_3}{k_4})$
Binding Potential (BP) $BP = \frac{B_{max}}{K_D}$	It is the ratio of B_{max} to K_D. B_{max} is the total density (concentration) of receptors in a sample of tissue. K_D is the inverse of the affinity of ligand binding.	$BP = \frac{k_3}{k_4}$
Unidirectional uptake rate constant (Ki)	Net inward transport and trapping of the radiotracer in tissue.	$K_i = \frac{K_1k_3}{k_2 + k_3}$

Table 1. Common macroparameters obtained from kinetic modelling.

To be able to solve our models more easily, we can do some approximations. Most radiotracers follow a two-tissue approach. In this approximation, the free tissue and non-specific binding are included in the same compartment (the sum is called non-displaceable radioligand). Thanks to

these assumptions, the models is reduced to two equations and three compartments, and we can estimate the V_T and BP with the equations in Table 1.

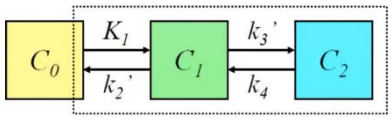

C_0(t): blood radiotracer concentration
C_1(t): free concentration in tissue + non-specific
C_2(t): specific radiotracer concentration (binding)

Figure 8. Two-tissue compartmental model [26].

Some radiotracers such as [^{18}F] FDG follow an even simplified kinetic that is derived from this model. We assume that k_4=0 (irreversibility conditions), which means that everything that binds and enters the specific radiotracer uptake compartment doesn't unbind [26]. This simplifies the calculations, and it is easier to estimate some macroparameters.

2.5 PET analysis methods

Compartmental models are the gold standard of kinetic modelling. However, as the complexity of the model increases, also increases the difficulty and complexity with the resolution of these equations. That's why there is a range of different approaches developed from the differential equations of the compartmental models [17]. The following are some of the most used methods in PET analysis.

Spectral analysis (SA)

Outcome	PET scan	Input function
K_i, V_T, number of compartments	Dynamic	Arterial plasma

Like compartmental models, SA describes the kinetics of the radiopharmaceutical using homogeneous compartments, but there is no need to know the number of compartments; SA can instead be used to estimate the number of compartments. Therefore, SA can be used for selecting or validating a compartmental model [28].

Standardized Uptake Value (SUV)

Outcome	PET scan	Input function
SUV	Static	Injected dose

This is a widely used PET quantifier, calculated through the following formula:

$$SUV(t) = \frac{C(t)}{ID/BW}$$

- C(t): Concentration of the radiotracer.
- ID: Injected dose.
- BW: body weight.

Equation 2. Formula to obtain the SUV.

SUV only works for static scanning, or for measuring the value at a specific point in time. It requires information about the injected dose and body weight of the subject. SUV can be considered a correct measure only if the radiotracer is very specific and/or blood radiotracer concentration is low and/or free tissue radiotracer concentration is low [29].

Standardized Uptake Value Ratio (SUVR)

Outcome	PET scan	Input function
SUVR	Static	Reference region

A more efficient static approach than SUV is the SUV ratio (SUVR). For this approach, we define a reference region and perform the ratio between the target and reference regions:

$$SUV_r = \frac{SUV_{target}}{SUV_{reference}}$$

Equation 3. Formula to obtain the SUVR.

When divided, the injected dose and body weight cancel from both SUVs, so the remaining equation is just the ratio between the concentrations of the target and reference regions.

The SUVR is a more robust method than the SUV because it does not require cross-calibration of PET scanner and dose calibration, so it allows a better comparison between images acquired in different conditions. There are problems, too: optimal reference tissue is not always available, and the data from reference tissue may be noisy because of the low radiotracer uptake [30].

Multiple-time graphical analysis (MTGA)

Outcome	PET scan	Input function
Ki, VT, BP, DVR	Dynamic	Reference region

In multiple-time graphical analysis, the radiopharmaceutical concentration curves of the region of interest and the reference region are transformed and combined into a single curve that approaches linearity when certain conditions are reached. The data can be plotted in a graph and fitted to the linear phase to obtain the slope of the line. This slope represents the parameter of interest we want to get (K_i, DVR) [31].

These methods have been developed to be used in both reversible and irreversible radiotracers. For the condition of irreversibility, the **Patlak plot** is used, which provides the rate constant Ki, whereas for reversible radiotracers models the **Logan plot** is used, which will provide us with the V_T, BP, and Distribution Volume Ratio (DVR).

Reference region input compartmental models

Outcome	PET scan	Input function
BP	Dynamic	Reference region

There are compartmental models that use a reference tissue instead of plasma sampling as the input function and are aimed mostly at reversible binding. While many models are usually applied to dynamic PET data collected after injection of one radiopharmaceutical, these models can be extended to dual-radiopharmaceutical (dual-tracer) PET studies, where two radiopharmaceuticals targeting different transmitter systems are injected [32]. Simplified reference tissue models (SRTM) and multilinear reference tissue models (MRTM) are examples of these models.

2.6 18F-PI-2620 in PET-tau quantification

As mentioned in the introduction, 18F-PI-2620 is the PET radiotracer we are focusing on in this project. There are already several studies with this radiotracer. For this project, I have selected several articles from the literature to find out the characteristics of the studies made with this radiotracer and the quantification methodology they use, so I can elaborate mine according to the characteristics of the radiotracer. The selected studies are included in the references of the project [6], [33], [34], [35], [36], [37], [38], [39], [40], [41], [42], [43], [44].

In the annexes of the project there are different tables that summarize the information about these studies. Most of the studies are aimed at PET-tau imaging, using 18F-PI-2620 as a potential biomarker for neurodegenerative diseases and tauopathies such as AD, PSP, mild cognitive impairment (MCI) and corticobasal syndrome (CBS). Several studies evaluate the differences between different brain pathologies, as well as comparing them with cognitive normal individuals, while others compare 18F-PI-2620 with other radiotracers.

❖ Image acquisition

The acquisition is almost always made in a PET/CT scanner, although PET/MRI scanners are also relevant. Sometimes, brain CT images are acquired for attenuation correction. The type of acquisition is usually dynamic, which is expected considering dynamic studies are better when we are evaluating a new radiotracer.

The injected dose varies considerably between studies, but plenty of them are around 185 MBq. For most dynamic studies, the acquisition time starts at the time of injection, and it is acquired for 60 minutes with 5-minute time frames. Others go up for 90, 120, and even 180 minutes. On the other hand, for static studies, the acquisition starts 60 minutes after the injection, lasting 30 minutes.

❖ Coregistration

Coregistration is a are very important step before quantification. Usually, brain PET images are coregistered with an MRI image and are then normalized into the MNI space. Most of them use the PNEURO pipeline in the software PMOD to delimitate the VOIs. Another relevant software for the segmentation of VOIs is FreeSurfer. The most used atlases to extract the regions of interest are the Hammers atlas and the Brainnetome atlas, with relevant regions such as the putamen, globus pallidus internus/externus, hippocampus and fusiform gyrus amongst many more.

❖ Quantification

For the quantification of the images, most studies use PMOD, a widely known commercial software for PET quantification. Others use FreeSurfer and FSL. The extracted parameters are mostly the Standardized Uptake Value Ratio (SUVR) and the Distribution Volume Ratio (DVR). SUVR is only extracted from static studies, so to calculate it they usually do the mean of the SUVR in different time frames, or they average different frames to create a static image. Usually, to extract the DVR they use the Logan graphical plot method, which is a non-invasive method, using the cerebellum as the reference region. Others use invasive methods that require blood sampling, or some less known non-invasive methods such as SRTM and MRTM.

3. Market analysis

In the field of neurology there is an increasing need for image processing tools to help the diagnosis and monitoring of patients with neurodegenerative diseases in an objective way. As our technology evolves, humans keep living longer, and we keep finding out new cognitive disorders, and imaging tests are one of the main methods for their detection.

This project is aimed at the healthcare sector, mainly to neurologists, radiologists, and nuclear medicine specialists. Medical centres are always looking for new advanced technologies to improve the diagnostic precision and attention quality to their patients. PSP is a rare neurodegenerative disease, with a prevalence of around 5-7 in 100.000 inhabitants [45], whose diagnosis in the early stages is still challenging. PSP can initiate with symptoms and signs resembling other parkinsonisms or cognitive disorders. Definite diagnosis is possible only post-mortem, and in the absence of a reliable biomarker, diagnosis is still heavily based on clinical criteria and uncertain.

The search for biomarkers in PSP aims to improve diagnostic accuracy at an earlier stage of the disease, as well as to track disease progression. Finding effective methods to identify PSP in its early stages would allow early interventions, such as personalized treatment for managing the symptoms and the participation in clinical trials with the hope of improving the quality of life of the affected population, as well as looking for a treatment of the disease.

Disease detection of 4R tauopathies in vivo have recently shown encouraging findings. The growing development of PET tau imaging has shown promising results in AD with 1st generation radiotracers [3]. However, problems with off-target binding and increased uptake in synucleinopathies have arose. The recent development of 2nd generation PET tau tracers has shown lower off-target binding and potential for non-AD tauopathies, which include PSP. A cross-sectional multicentre study with 60 PSP patients has demonstrated the potential utility of 18F-PI-2620, capable of binding to 4R tau isoform in all subcortical PSP target regions [46].

This search for a useful detection method in PSP is why we will develop and validate a robust and accurate quantification tool for the evaluation of PET images with 18F-PI-2620.

Given significant continued efforts with dynamic imaging, particularly in PET, there exist many software packages that aim to perform kinetic modelling and estimate parameters of interest. Most kinetic modelling efforts have been historically in brain and cardiac applications [17]. The development of more sophisticated algorithms that allow better segmentation and image analysis keeps improving the precision and reproducibility of the results. Moreover, the integration of artificial intelligence (AI) and machine learning (ML) has opened plenty of possibilities in this field.

There are plenty of software that allow the analysis of PET data. Most of them can be found referenced on the NMMItools website (nmmitools.org), an up-to-date online reference website for software tools to simulate, reconstruct and analyse synthetic or real data related to Nuclear Medicine and Molecular Imaging (NMMI) studies [47]. Many more can be found in *Wang G (2020)* [17], which compiles a list of the different software for kinetic modeling and parametric imaging.

Most software allow the coregistration and normalization to the MNI space of PET images using atlases. Many also perform the quantification and creation of parametric images by using reference tissue models. The code we are creating must fulfil these steps, so we can take advantage of already existing open-source software for this purpose since the proliferation of open-source software has democratized the accessibility to advanced tools of image processing.

ML also offers a new way to quantify PET images that is more precise and robust than traditional methods. ML methods can be trained in great groups of data of PET images and radiotracers, which allows the learning of the complex relationships between images and radiotracer concentrations. For instance, *Kang (2015)* employed a random forest to predict the full dose PET from low dose PET and MR images [48]. They used characteristics of each image to construct specific models for each tissue and refined the prediction to improve the precision.

Concerning deep learning (DL), there are more complex approaches that can predict PET images with a complete dose from PET images with a low dose and MRI, using convolutional neural networks (CNNs), which mimic the functioning of human brains. *Xiang (2017)* proposed a deep auto-context CNN to predict full-count PET images based on local patches in low-count PET and MR images [49].

The future of PET image quantification is promising, with continuous advancements in processing algorithms and reconstruction techniques. It is expected that we will have greater precision and sensibility in the measurement of the metabolic activity in the brain and radiotracer distribution, which will allow earlier illness detection and more precise treatments.

4. Concept engineering

The main goal of the project is to create a software using Python, which englobes tasks from the preprocessing of the images to the analysis of the results. In this section, we will now go through all the functionalities our code must have and how will we approach them.

❖ **Preprocessing**

Before quantifying the image, we must go through some preprocessing. Since we are working with brain images, we must correctly coregister them into an anatomical image and normalize them into the standard space. This way we will be able to compare different subjects in the same space and to distinguish the different brain regions with the help of an atlas. To load the images in our Python code we are going to use the library NiBabel, which allows access to read and write to common neuroimaging formats, including NIfTI, which is the format our images are in [50].

If we want to normalize the subjects into the MNI space, we need to use the anatomical reference images. We will create a first transformation by coregistering each subject's static PET (average of the six frames) to their corresponding MRI (Figure 9). Then, we create a new transformation by coregistering the MRI anatomical image to the MNI space using a template (Figure 9). We will use the MNI152 standard-space T1-weighted average structural template image from FSL, with 1 mm^3 resolution [51].

By applying these two transformations to the dynamic PET image (Figure 9), we will have the PET images coregistered to the standard space, in 4D. To perform these transformations, there are several Python packages available. We will use a library named ANTsPy (Advanced Normalization Tools in Python). ANTsPy is a Python library that wraps the C++ biomedical image processing library ANTs, matches much of the statistical capabilities of ANTsR, and allows seamless integration with NumPy, scikit-learn, and the Python environment [52]. It allows the coregistration of images with simple functions that are well-documented.

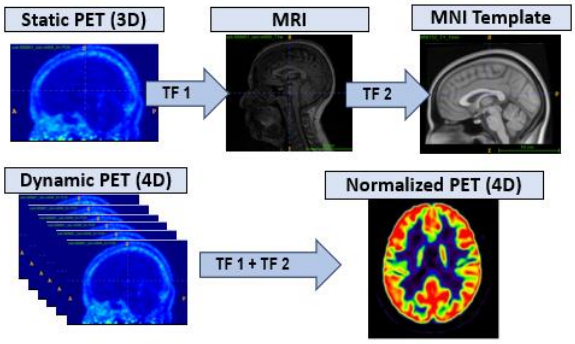

Figure 9. Diagram of the coregistration workflow. Normalized PET reference: [53].

By coregistering the images to the template, we won't need to generate brain masks of the PET images (which serves to eliminate the skull from the images), as we can just use the template's mask for selecting the whole brain and the atlas to select the different regions.

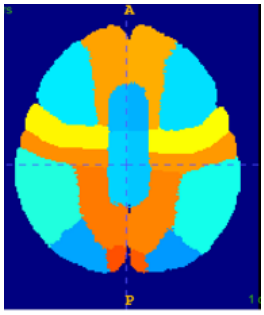

Figure 10. Hammers atlas, axial view in ITK-Snap.

After having applied both transformations to the dynamic PET images, we will be able to segment the regions in the brain with an atlas. We are going to use the Hammers atlas, which, as we have seen in the *Background* section, is very popular in 18F-PI-2620 studies and is available for free on the internet [54]. This atlas comes with an image in HDR format that has an intensity number (label) for each region (Figure 10), and a CSV file that contains the information about each label (region's name, region's hemisphere, and region's lobe). The atlas we are using contains 33 regions, divided into the left and right hemispheres, giving a total of 66 regions. For future PSP studies, the regions might have to be adjusted, but for now we will use this atlas for testing.

Each voxel intensity in a PET image corresponds to the radiotracer concentration in that point. These values can be extracted using the NiBabel Python library and be used to plot the time-activity curves (TACs). For each region in the atlas, we can compute the mean radiotracer uptake for each time frame and plot the regional radioactivity levels as a function of time. Since our images have 6 time frames, that's how many points each TAC will have.

Another step that is usually done in PET image preprocessing is partial volume correction (PVC) to correct the partial volume effect (PVE), which degrades the quantitative accuracy of PET images. Because of PVE, the intensity of a particular voxel reflects the tracer concentration not only of the tissue within that voxel but also the surrounding area. PVC techniques are designed to correct the spillover effect caused by the poor spatial resolution of PET images [55]. Since it is not an essential

step to fulfil our goal and our time is limited, we won't be implementing PVC and will be focusing more on the quantification. However, we leave PVC and other methods to improve the quality of the image as possible future implementations of the software.

❖ Quantification

In the *Background* section, we have seen different methods for the analysis of PET data. From previous studies with 18F-PI-2620, we know that the most common studied parameters are **Standardized Uptake Value Ratio (SUVR)** and the **Distribution Volume Ratio (DVR)**. These are the two parameters we will be using for the quantification.

SUVR is an approach aimed at static scanning. We could use the average static images provided in the image set, but we want all our quantification process to be based on using the dynamic images directly, so we will create static images for each subject by adding up all the time frames in the coregistered dynamic images. SUVR consists of normalizing the radioactivity concentration to a reference region, making it so images acquired in different conditions (injected dose, scanner calibration, etc.) can be compared. It uses a reference region as input function, which makes it a good option, since we don't have any information about plasma sampling in our subjects. For the reference region, we will use the cerebellum (both left and right joined), since is the most used in previous studies with 18F-PI-2620. In Hammers atlas, the whole cerebellum corresponds to regions 17 and 18. Although this methodology is aimed at dynamic images, SUVR will be very useful to assess the validity of the software by comparing the results with these values with the DVR.

The DVR is usually obtained through the Logan plot graphical method in single-dose studies of reversible radiotracers, which our case. It is aimed at dynamic scanning, so it might be a more efficient approach than the SUVR. It also uses a reference region as the input function, so it is also a viable method.

The Logan plot is based on the assumption that the tracer kinetics in the tissue of interest can be described by a two-tissue compartment model [31]. The DVR is the ratio between the distribution volume in the target region to that in the reference region. It is also related to the binding potential through Equation 4:

$$BP = \frac{V_T}{V_T^{ref}} - 1 = DVR - 1$$

Equation 4. Relationship between the BP, V_T and DVR

The Logan plot is constructed by doing a transformation and combination of the radiotracer time-activity curves (TACs) in the target region and the reference region. The TACs show the radiotracer distribution in a region through time. When we combine the TACs of a target region and a reference region with a specific formula, we produce a new equation that represents a curve that approaches linearity (Figure 11). This equation must include the parameter of interest (DVR) we are interested in measuring as the slope. Since we are talking about a linear curve, said parameter can be obtained through a linear regression [56]. Equation 5 is the equation used for the Logan plot when a reference region is available (no plasma sampling), where the slope of the linear portion of the Logan plot is equal to the DVR, and linearity is achieved after the intercept (Int) is effectively

constant [56]. C_{ref} is the concentration in the reference region, and C_{ROI} the concentration in the target region.

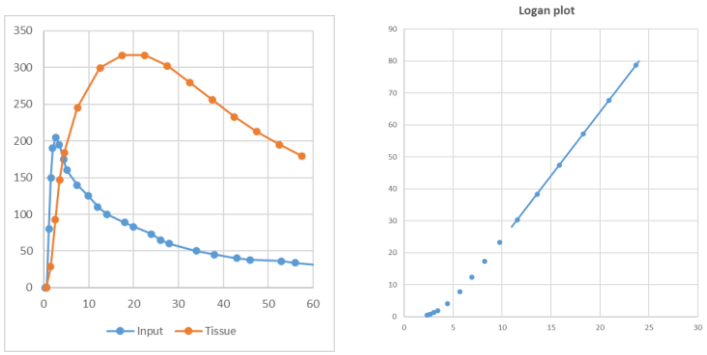

Figure 11. Logan plot simulation from turkupetcentre.net [57]. On the left, the TAC of the reference (input) and target tissues, where the x axis represents time, and the y axis is the radiotracer concentration. On the right, the Logan plot obtained from transforming and combining the TACs.

$$\frac{\int_0^T C_{ROI}(t)dt}{C_{ROI}(T)} = DVR \cdot \frac{\int_0^T C_{ref}(t)dt}{C_{ROI}(T)} + Int'$$

Equation 5. Logan plot equation to obtain a linear function.

To save time and work, I looked for an already existing software that uses this Logan formula, so I can use their algorithm in my code. Thus, we are looking for a free, open-source software able to perform the Logan method. Also, it should be implemented in Python, so we don't have to translate it. Table 2 shows multiple available open-source software that are aimed at dynamic PET quantification and kinetic modelling. Next page has a brief description of some of the most popular.

Name	Use	Language	Can perform Logan
Imlook4d	Free	MatLab	No
Kinfitr	Free	R	Yes
MAGIA	Free	MatLab	Yes
PMOD	Commercial	Java	Yes
APPIAN	**Free**	**Python**	**Yes**
QModeling	Free	MatLab	Yes
FreeSurfer	Free	C++	Yes
TriDFusion	Free	MatLab	No
NiftyPET	Free	Python	No
Pet2mri	Free	Python	No
DynamicPET	Free	Python	No
Quality-assurance	Free	Python	No
NiftyPAD	**Free**	**Python**	**Yes**
Tacmagic	Free	R	Yes

Table 2. Open-source software for dynamic PET quantification.

Dynamic PET

Open-source	Python	Free

Dynamic PET is designed for voxel-wise analysis of reconstructed dynamic positron emission tomography (PET) scans and also supports regional analysis. It does a reference tissue-based modelling: SUVR and SRTM [80].

MAGIA

Open-source	MatLab	Free

Magia uses standardized methods to produce parameter estimates describing the kinetics of a tracer from brain PET studies. For reference region studies, Magia aligns the frames, coregisters the PET image to a specified MRI, produces a reference region, calculates parametric images and ROI level parameter estimates using the specified model, and finally normalizes and smooths the parametric images [79].

NiftyPAD

Open-source	Python	Free

NiftyPAD was designed to support several important features which are not available in other existing software packages for kinetic modelling and does an analysis of static, dynamic, and dual-time window PET data. NiftyPAD provides a group of reference-based kinetic models such as Logan, STRM, and MRTM [59].

QModeling

Open-source*	MatLab	Free

QModeling is a multi-platform toolbox for the SPM software to fit reference-region kinetic models (currently supporting SRTM, SRTM2, Patlak Reference, and Logan Reference Plots) to dynamic PET imaging data [81].

*Requires SPM

APPIAN

Open-source	Python	Free

APPIAN (Automated Pipeline for PET Image Analysis) is an automated software pipeline for analyzing PET images in conjunction with MRI. The goal of APPIAN is to make PET tracer kinetic data analysis easy for users with moderate computing skills and to facilitate reproducible research [58].

PMOD

Source code upon license purchase	Java	Commercial

PMOD includes two toolboxes (PKIN and PXMOD) that allow for kinetic modelling. The results are images, namely parametric maps, showing the value of a model parameter in each image pixel. Hereby, quantitative tissue properties are visualized and can easily be compared against information from other sources, such as autoradiography [78].

Kinfitr

Open-source	R	Free

The goal of this package is to equip PET modellers with great flexibility, while simultaneously making it easier to produce, present and share their results in a highly transparent manner using R and its ecosystem of tools for computational reproducibility. It uses several reference region models (including Logan), as well as models requiring arterial input [76].

FreeSurfer

Open-source	C++	Free

PETSurfer provides a set of tools within *FreeSurfer* for end-to-end integrated MRI-PET analysis, including motion correction, PET-MRI registration, reference region kinetic modeling (MRTM1, MRTM2, Logan), partial volume correction (PVC), and group analysis in ROI, volume, and surface spaces [77].

According to Table 2, there are only two options that fulfil all the requirements. These are **APPIAN** and **NiftyPAD**. APPIAN is currently only available through Docker, a platform for creating containers that package a given software in a complete filesystem that contains everything it needs to run and ensures that the software can always be run in the same environment [58], which makes it less suitable for tailoring the pipeline.

On the other hand, NiftyPAD, although it is recent and lacks proper documentation, in *Jiao, J (2023)* [59], we can learn the different things we can do with this pipeline and shows to provide very accurate results. Also, on its GitHub page, apart from being able to see all the functions, we find some examples of how to implement some of them, including the Logan model. Thus, we are going to use the help of NiftyPAD for the computation of the DVR.

NiftyPAD is a freely available, open-source, Python-based software package for the analysis of both static and dynamic PET data. The package has been proven to be versatile, flexible, and to produce comparable results with established software packages for the quantification of dynamic PET data (specifically QModeling and PPET). PAD stands for package for quantitative analysis of dynamic PET data [59].

NiftyPAD supports images in NIfTI format, so we won't encounter any issues. It provides several tools for the analysis of PET images, but what we are interested in, and will focus on during this section, is the quantification of dynamic PET data without the need for blood sampling using the Logan method.

The Logan method in NiftyPAD is based on *Logan, J. (1996)* [56]. It uses the radioactivity concentrations of the region of interest and the reference region through time to generate a linear curve with the DVR as the slope. To do so, they offer two different functions that use Equation 6 (a) and (b), respectively, where C_R is the concentration in the reference region, C_T is the concentration in the target region, and k2' is a predefined parameter called the efflux constant, which represents the tissue-to-plasma radioligand transfer in a non-receptor region (reference region):

$$(a)\ \frac{\int_0^T C_T(t)dt}{C_T(T)} = DVR\frac{\int_0^T C_R(t)dt}{C_T(T)} + int' \qquad (b)\ \frac{\int_0^T C_T(t)dt}{C_T(T)} = DVR\frac{\int_0^T C_R(t)dt + C_R(t)/k'_2}{C_T(T)} + int'$$

Equation 6. Equations used for Logan in NiftyPAD (a) without k2' and (b) with k2'.

Since we don't have any information about the k2' in our images, we will just be using the first model, with the function from NiftyPAD called *logan_ref*. With this function, we will be able to get the Logan plot for each desired region, whose slope is the DVR.

With all of this, we will be able to analyse our results by comparing the SUVR and DVR in different regions and the different subject groups (control, aDS, dDS), and create parametric images to evaluate the radiotracer distribution in our images.

Every step we have mentioned must be part of a unified Python code that constitutes the software. The code will be divided into different scripts, each of them with a concrete task for the quantification process.

5. Detailed engineering

The focus of this project has been to create a software with Python to quantify dynamic PET images. In this section, I will describe the goal and functioning of each of the different scripts in the code and do a detailed explanation of their functions in a simplified manner, and the results they generate when used with a set of images. The code has been uploaded in a GitHub repository for future use in the CIBER-BBN project. Since there is a clinical trial and a bigger project behind this work, it is in a private repository, which includes the 8 scripts used for the software's code and a README file with information about the code. This section is also aimed to be a guide for those who might use the software.

The Python libraries imported for this code are ANTsPy, NiBabel, Pandas, SciPy, NumPy, NiftyPAD, OS, Matplotlib, Seaborn, SciKit and JSON, and have been used thanks to their documentation online [50], [60], [61], [62], [63], [64], [65], [66], [67], [68], [69].

Currently, ANTsPy only works in the Linux operating system. So, to code it and test the scripts that use this library, I used a remote connection to a local computer in the biophysics lab in the faculty, since it uses this operative system.

Each script contains a function called `main`[3], which is the function that executes when running the script. Inside this function, the user must define some parameters (Table 3), such as paths to files or the desire to perform certain operations. The `main` function calls all the other functions of the script in an ordered manner so that everything is done correctly.

`path_in`	*String*. Path to the folder with all the images for all subjects.
`norm_pet_path`	*String.* Path to the folder with the normalized dynamic PET images.
`template_path`	*String.* Path to the template.
`atlas_csv_path`	*String.* Path to the atlas csv file.
`atlas_img_path`	*String.* Path to the atlas NIfTI file.
`mask_path`	*String.* Path to the brain mask of the template.
`rois`	*List/String.* Specifies the regions you want to analyze (List or "all").
`reference_region_labels`	*List.* The labels of the reference region.
`fig`	*Boolean.* Specifies if you want to save plots created by the function.
`csv`	*Boolean.* Specifies if you want to save the results as a csv file.
`output_path`	*String.* Path to the folder where the generated files are saved.

Table 3. The parameters the user defines serve as inputs for the functions in the code. These are the most relevant, but some scripts have some additional ones or similar ones with variations in the names.

An important function in all the scripts is the one called **`files`**. This function organizes all the images to analyse in a DataFrame called `files_df` that has a subject for each row, with the subject's name and the paths to their images. Each script will have a `files` function modified according to the files that we want to use, so that each step of the process can be performed to all the subjects.

[3] I will be using `this format` to refer to variables, functions, etc. from the code.

5.1 Coregistration and normalization

The first script (named *coreg*) has the objective of coregistering the dynamic PET images to their corresponding anatomical images (MRI) and normalize them into the MNI space.

❖ MRI coregister

After using the `files` function to organize each subject's images, the function **`petdyn_2_mri`**, will perform a registration of the dynamic PET image to the MRI image using an affine transform. This transformation preserves lines and parallelism, but not necessarily Euclidean distances and angles. Since the PET and anatomical images are from the same brain, this is the transformation we must apply.

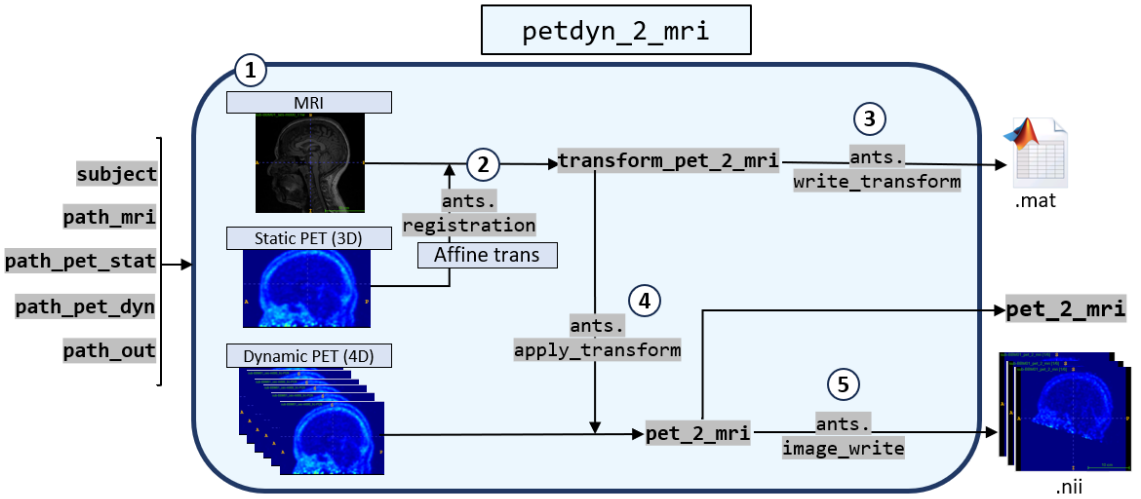

Figure 12. Diagram of the *petdyn_2_mri* function.

1	The MRI, static PET (created by averaging the time frames in the dynamic one) and dynamic PET images are loaded.
2	Using the `ants.registration` function from ANTsPy, an affine transformation to the static PET image is performed, with the MRI being the fixed image.
3	The transformation matrix is saved as a .mat file using `ants.write_transform` inside a folder named as the subject id in `path_out`.
4	The transformation is now applied to the dynamic PET image using `ants.apply_transform`. We name this image `pet_2_mri`.
5	The coregistered image is saved as a NIfTI file in the same folder as the transformation, using `ants.image_write`.

Returns	`pet_2_mri`	*ANTsImage*. Image of the 4D PET coregistered to MRI.

Table 4. Step-by-step explanation of the *petdyn_2_mri* function.

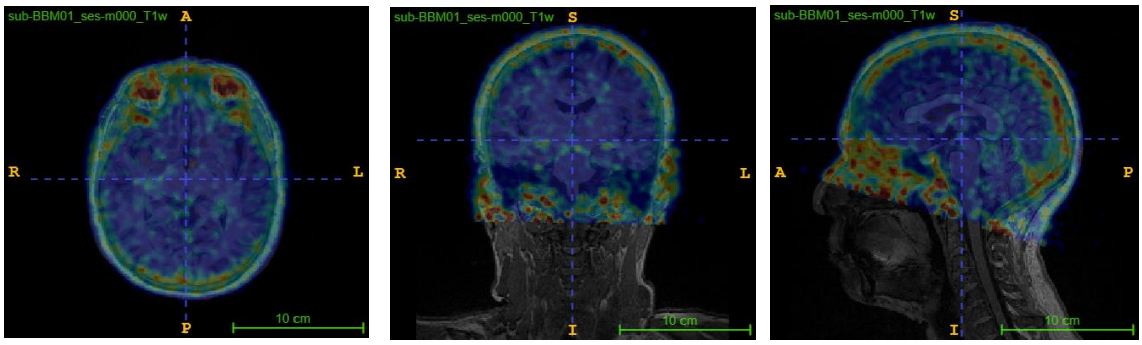

Figure 13. Axial, coronal and sagittal planes of the coregistered dynamic PET image overlayed to the MRI image, visualized in ITK-Snap (subject BBM01, time frame 1).

❖ Normalization to template (MNI)

The previously coregistered image will be used in the next function, called **`petdyn_2_template`**, and will coregister it to the MNI template, using a Symmetrical Normalization (SyN), so we will have all the subjects in the same space. This transformation involves aligning and scaling images to a reference space while preserving symmetry and anatomical correspondence. We use a transformation from the MRI to the template since we can only create transformations to a template if we do so from anatomical images. This transformation can then be applied to the PET image which is already coregistered to the MRI space.

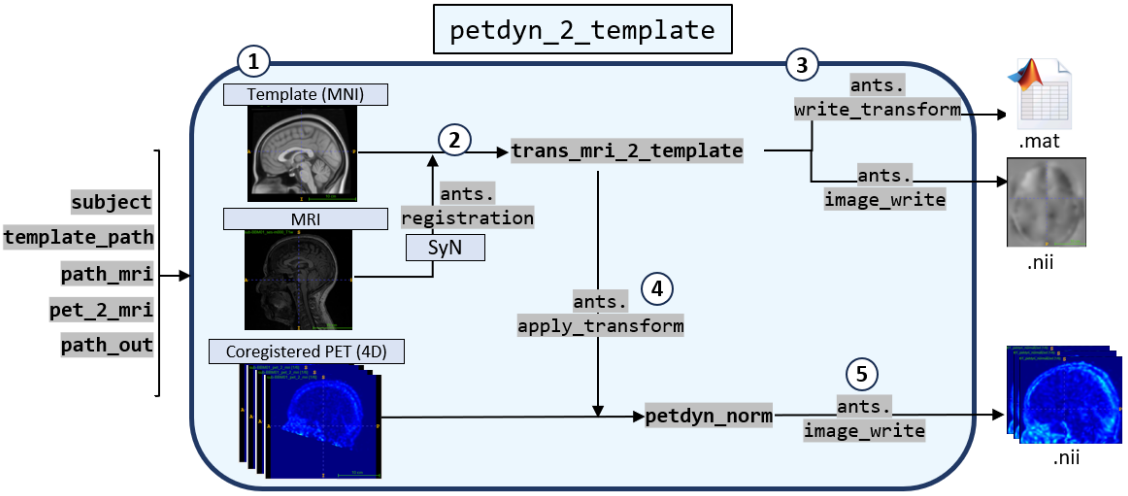

Figure 14. Diagram of the *petdyn_2_template* function.

1	The template, MRI image, and previously coregistered PET image are loaded.
2	Using `ants.registration`, a Symmetrical Normalization is applied to the MRI image, with the template being the fixed image.
3	The transformation matrix and a warped NIfTI image (represents how the image has been deformed to align with the other) are saved in `path_out`.
4	The transformation is applied to the previously coregistered PET image, so we coregister it again but this time to the MNI space.
5	The new coregistered image is saved with the transformations in NIfTI format. We have a 4D PET image normalized to the MNI space.

Table 5. Step-by-step explanation of the *petdyn_2_template* function.

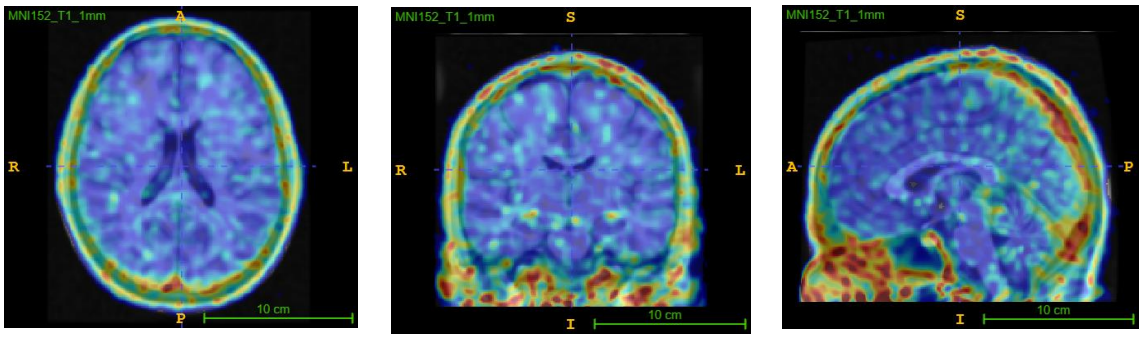

Figure 15. Axial, coronal and sagittal planes of a normalized PET image overlayed to the MNI template visualized in ITK-Snap (subject BBM01, time frame).

5.2 Time-activity curves

The next step for quantification is to generate the time-activity curves of each subject. TACs show the radiotracer distribution in the brain as a function of time and are crucial to apply the quantification models we are going to use (Logan and SUVR). The main goal of this script (named *tacs*) is to obtain a DataFrame that contains, for each subject, each region, and each time frame, the mean radiotracer uptake. We will also include the median and standard deviation. The results can be saved in CSV files and in plots.

❖ Regional TACs

The first function is called `time_activity_curves`. It uses the DataFrame created in `files` to create a dictionary that contains a DataFrame for each subject with the information about the activity in each region and time frame.

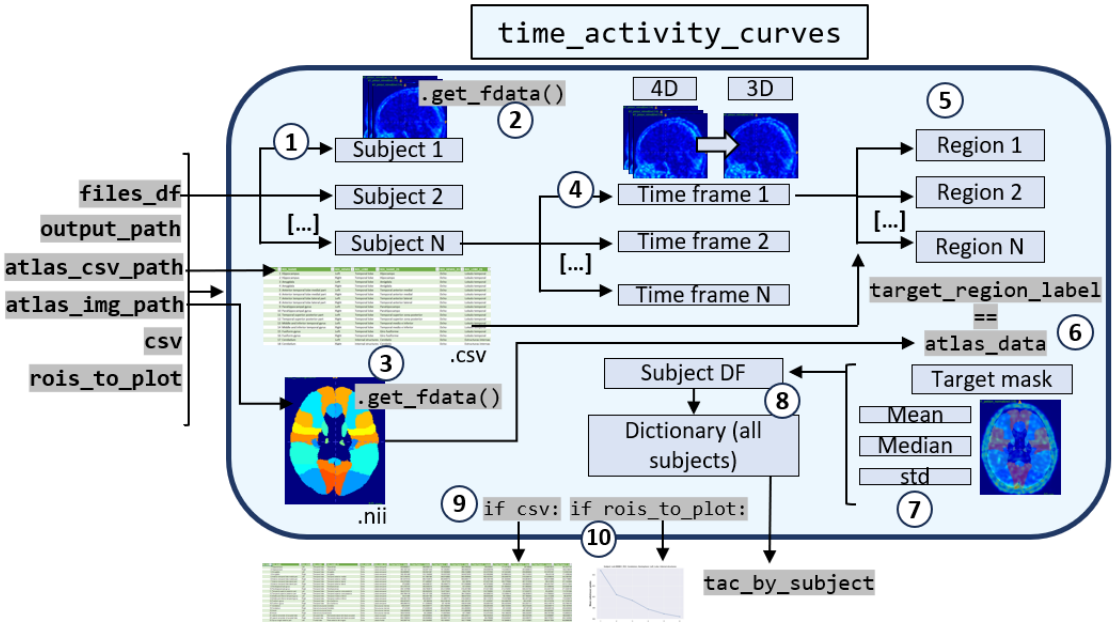

Figure 16. Diagram of the *time_activity_curves* function.

1	From `files_df` we obtain the 4D PET normalized image of each subject.
2	Using the `get_fdata()` function from *NiBabel*, we get an array with the values representing the intensity of each voxel (radiotracer uptake).

3	We load the CSV file containing the information about the ROIs in the atlas, and also the atlas NIfTI image, and access the numbers representing each ROI.
4	For each subject, we divide the 4D image into the 3D images that compose it, one for each time frame.
5	For each time frame, we iterate through all the regions that appear in the atlas CSV file.
6	For each region, we compare the label of the region with the data in the atlas. We get the voxel intensities of our PET image in each region defined by the atlas image.
7	We compute the mean, median and standard deviation of the voxel intensity in each region.
8	We put this information into a dictionary with a DataFrame for each subject, which will contain the mean, median and std for each ROI in each time frame.
9	If `csv` is specified to be True, each DataFrame will be saved as a CSV file in `output_path`.
10	Then, if the user specifies it, it calls the function `generate_plots` and saves a plot for each specified ROI in `rois_to_plot` for all subjects that will be saved in `output_path`.
Returns	`tacs_by_subject`	*Dictionary.* Contains a DataFrame for each subject with the mean, median and std for each time frame and region.

Table 6. Step-by-step explanation of the *time_activity_curves* function.

Figure 17 shows part of the CSV file created for a subject, where we can see the mean, median and standard deviation of the different regions and time frames.

ROI_NUM	ROI_NAME	ROI_HEMIS	ROI_LOBE	('Time Frame 1', 'mean')	('Time Frame 1', 'median')	('Time Frame 1', 'sd')
1	Hippocampus	Left	Temporal lobe	1688,841459	1647,515686	348,7417175
2	Hippocampus	Right	Temporal lobe	1737,812229	1721,369751	344,8033128
3	Amygdala	Left	Temporal lobe	1964,970641	1931,172119	449,8012904
4	Amygdala	Right	Temporal lobe	2220,22497	2175,745117	566,393959
5	Anterior temporal lobe medial part	Left	Temporal lobe	1535,170784	1463,189697	375,7989059
6	Anterior temporal lobe medial part	Right	Temporal lobe	1474,500096	1403,2995	451,9496891
7	Anterior temporal lobe lateral part	Left	Temporal lobe	1228,759059	1216,614929	220,5322114
8	Anterior temporal lobe lateral part	Right	Temporal lobe	1178,952429	1152,403137	233,0947078
9	Parahippocampal gyrus	Left	Temporal lobe	1613,794971	1557,222534	452,6719647
10	Parahippocampal gyrus	Right	Temporal lobe	1731,378102	1696,983032	438,115852
11	Temporal superior posterior part	Left	Temporal lobe	1144,264971	1127,043091	198,4193206
12	Temporal superior posterior part	Right	Temporal lobe	1211,221837	1195,642944	273,4806531

Figure 17. CSV file created by the function. Since it is too large to fit entirely, here we see part of it, with the first 12 regions and the first time frame (subject D3553).

As seen in step 10, the function calls another function called **`generate_plots`** to plot the specified ROIs. This function simply gets the mean values for each time frame and plots them for each subject and region (Figure 18). We can see the radiotracer concentration decaying over time.

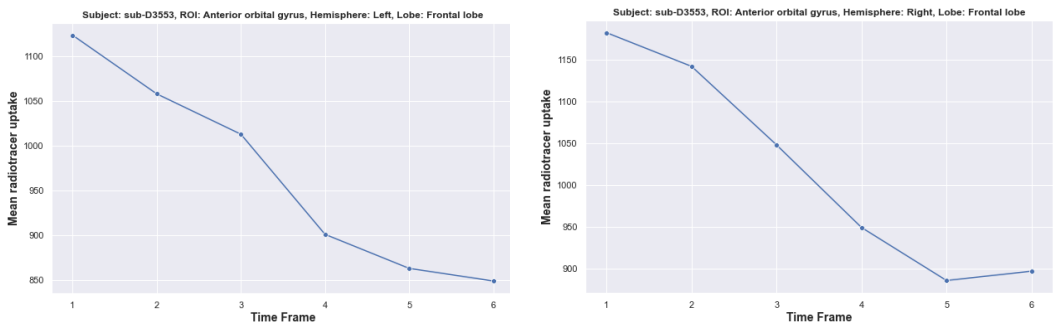

Figure 18. Plots generated by the function (anterior orbital gyrus left and right, subject D3553)

❖ Reference TAC

The last function in this part is `tac_ref`. This function serves to provide the TAC of the reference region for each subject, due to its importance in the upcoming quantification steps. It works very similarly to `time_activity_curves` but is less complex. It will just calculate the mean radiotracer uptake in the regions provided by the user in the input `reference_region_labels`. In our case, we used regions 17 and 18 from Hammers atlas, which correspond to the left and right sides of the cerebellum. The function will return a dictionary with an array for each subject, with the mean radiotracer uptake in the reference region for each time frame.

To make the reference region more efficient, it applies an erosion to the reference region, using the `binary_erosion` function from *SciPy*. Erosion is a morphological operation used in image processing to shrink the boundaries of regions in an image. This is done in case there are subjects where the coregister has moved a little the cerebellum and is getting radiotracer concentration where it isn't supposed to. The function applies one iteration, but we could apply more.

It is also worth mentioning that the atlas was modified to match the dimensions of our PET images in a previous script called *fix_atlas*. This doesn't affect in any way the data of the images, but is necessary so that we enable the comparison between them in the code. The dimensions might need to be resized with different values if another atlas is used, but it is not a problem at all.

5.3 SUVR

This script (named *suvr*) will perform several tasks aimed at using the SUVR method for quantification.

❖ Regional SUVRs

The first function is `suvr_static`. This function will add all the time frames from each 4D PET image into a 3D PET image, creating an averaged static image from our originally dynamic one. It will compute the SUVR of each specified ROI in this new static image and save the results in a CSV file and in a new NIfTI image with its regional SUVRs as the intensities.

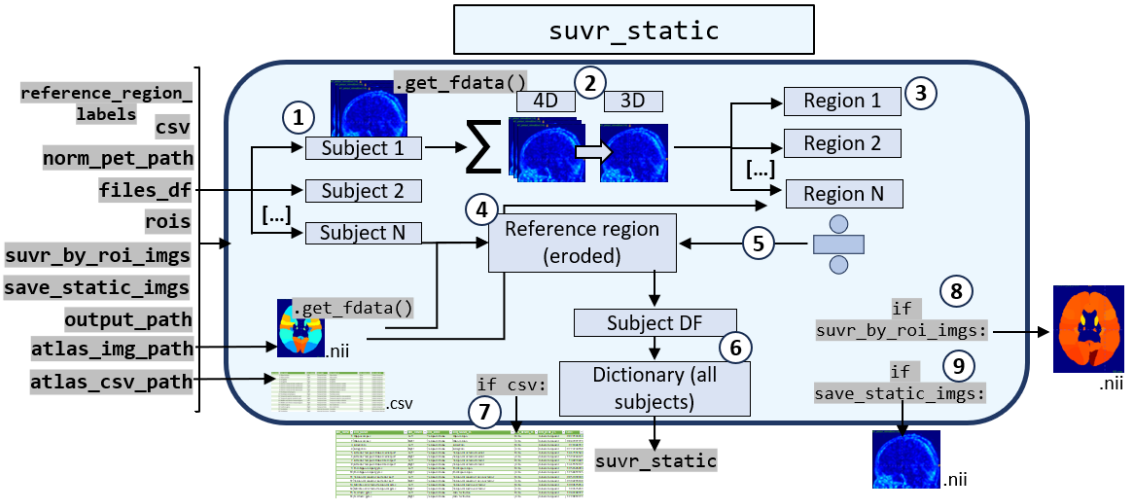

Figure 19. Diagram of the *suvr_static* function.

1	From the `files_df` input, get the dynamic PET image for each subject, and use the function `get_fdata` to get the intensity numbers of each voxel.
2	Add up all the frames in the 4D image to create a static 3D image for each subject.
3	With the help of the atlas, get a mask for each region, similarly to the `time_activity_curves` function.
4	Get a mask for the reference region of each subject as well, and apply an erosion, similarly to the `tac_ref` function.
5	Compute the SUVR of each specified ROI in the input `rois` by dividing it by the reference region.
6	Create a DataFrame for each subject with the SUVR of each ROI and append each DataFrame to a dictionary.
7	If `csv` is stated True, save each DataFrame as a csv file in `output_path`.
8	If `suvr_by_roi` is stated True, the function `rois_img_suvr` is called and saves the created images in `output_path`.
9	If `save_static_images` is stated True, the 3D static images are saved in `output_path`.

Returns	`suvr_static`	*Dictionary.* Contains a DataFrame for each subject. Each DataFrame has the SUVR for each ROI in the static image.

Table 7. Step-by-step explanation of the *suvr_static* function.

In step 8, if specified, the **`suvr_by_roi`** function is called. This function iterates through each subject's static image and, for each region, changes the intensity of the whole region so that is corresponds with its SUVR, creating a new brain image.

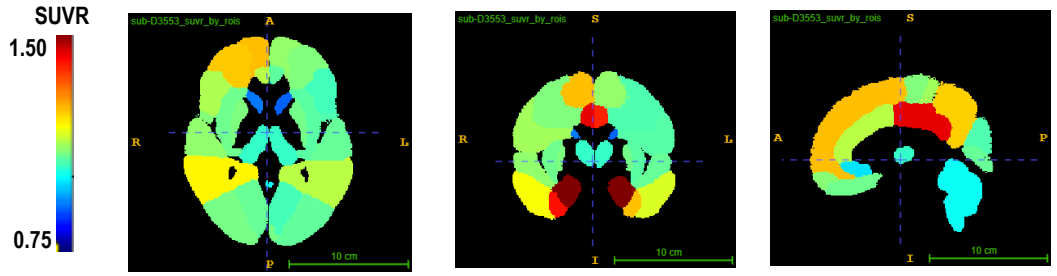

Figure 20. Axial, coronal and sagittal planes of an image created by the *suvr_by_roi* function (subject D3553), and the corresponding colour scale, visualized in ITK-Snap. Each region has its mean SUVR as the intensity.

ROI_NUM	ROI_NAME	ROI_HEMIS	ROI_LOBE	SUVR
1	Hippocampus	Left	Temporal lobe	1,5865
2	Hippocampus	Right	Temporal lobe	1,5860
3	Amygdala	Left	Temporal lobe	2,0474
4	Amygdala	Right	Temporal lobe	2,1088
5	Anterior temporal lobe medial part	Left	Temporal lobe	1,3910
6	Anterior temporal lobe medial part	Right	Temporal lobe	1,4224
7	Anterior temporal lobe lateral part	Left	Temporal lobe	1,1258
8	Anterior temporal lobe lateral part	Right	Temporal lobe	1,1357

Layer	Intensity
sub-...	1,391
atlas_modified	5

Figure 21. On the left, part of a CSV file created by the suvr_by_roi function, showing the first 8 regions and their mean SUVR (subject D3553). On the right, a screenshot of ITK-Snap while viewing the image in Figure 20, overlayed to the atlas, while clicking on region 5. We see how the intensity corresponds to the SUVR of region 5 in the CSV file.

Another function in this script is one called `suvr_per_frame`, which gets the SUVR values for each subject, ROI and time frame. It uses the TACs created previously and normalizes them by the reference region. It can save the results as CSV files and plots (using `generate_plots` from the previous script). This function is not much relevant for the results, so we won't get into detail.

❖ SUVR parametric images

The last function in this script is called `parametric_img_suvr` and it creates the SUVR parametric images. It will provide a parametric brain image for each subject where each voxel corresponds to the SUVR at that same point. It works similarly to the `suvr_static` function, but instead of iterating through all the regions in the atlas, it iterates through each voxel in the static brain image and normalizes each voxel's intensity by the mean intensity of the reference region. The images will be saved in NIfTI format in `output_path`. To avoid getting all the voxels of the image that are not part of the brain, we applied the brain mask of the template to the PET images.

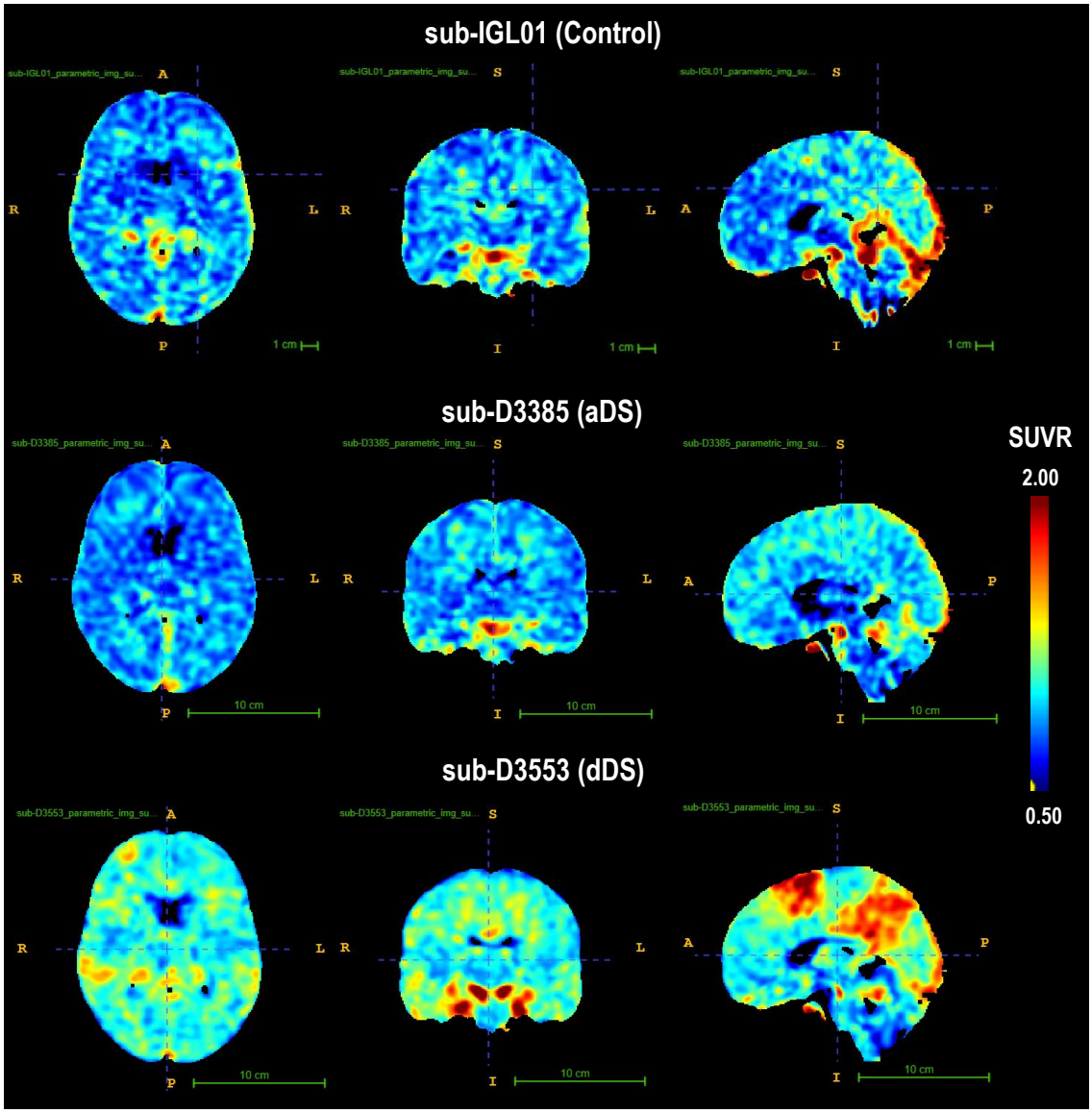

Figure 22. Axial, coronal and sagittal view of three different SUVR parametric images viewed in ITK-Snap, and the corresponding colour scale. Each image corresponds to a subject from one of the three groups. Clearly, there is a larger radiotracer uptake in the dDS subject, who has developed Alzheimer's.

5.4 Logan graphical method (DVR)

This script (named *dvr*) is the most complex one, but also the most crucial for our work. Here we will quantify the dynamic images using the Logan graphical method, which is a more suited method for dynamic images than the SUVR, and we will obtain the DVR for each subject and ROI, as well as parametric images.

❖ Obtaining the time intervals

First, we use the `dt_from_json` function. This function goes through the JSON file of each subject. JSON files are text files that contain information about the image acquisition, including the duration of each time frame. These files form part of the BIDs standard to keep information from the images that can't be stored in the image header. If the database is not designed in BIDS format, this required information should be stored and used from other files.

The function will return a dictionary with a double array for each subject (we will call it `dts`), containing the start and end times of each time frame. In our case, all subjects have 6 time frames of 300 seconds each, so all the arrays look like the one in Figure 23.

0	300	600	900	1200	1500
300	600	900	1200	1500	1800

Figure 23. Double array with start and end times of each time frame (screenshot from Python Spyder environment).

❖ Regional DVRs

The next function we call is the `dvr_values` function, which calculates the DVR for all ROIs and subjects. This function uses the `logan_ref` function from NiftyPAD, mentioned in *Concept Engineering*. However, I wanted to make some changes to the function so it could fit properly into our code. Since NiftyPAD gives free permission to use its functions, I put the `logan_ref` function into my script, modified it and called it `logan_niftypad`.

The inputs of this function are the TAC of the target region, the TAC of the reference region (input function), the array containing the start and finish times of each time frame, a vector that assigns a weight to each time frame (w), and the start and end times of the time range for the linear phase where the Logan plot will be applied.

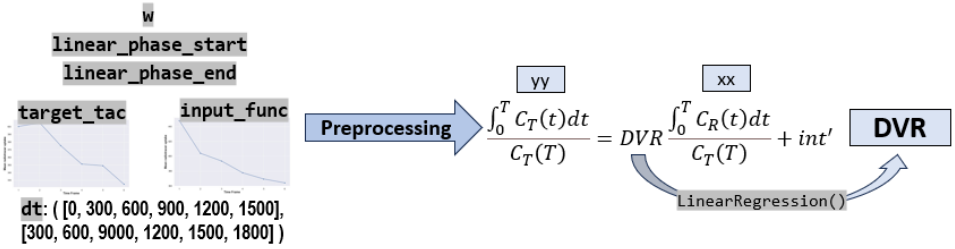

Figure 24. Diagram of the logan_niftypad function.

First, the function does a preprocessing of the data so it can perform correctly. If the time intervals dt have gaps (indicating non-uniform sampling), it fills those gaps using interpolation to ensure uniform time intervals. Also, it converts the time intervals (dt) to mean frame times and calculates the duration of each frame. It also adds a zero value and converts negative values to 0 in the tac

and input arrays. Finally, it interpolates the reference input function to match the time points of the time-activity curve.

Then, it computes the ratios (we will call them xx and yy) of the cumulated concentrations and concentrations (Figure 24). With these ratios, it uses the formula for obtaining the DVR through linear regression. The function will return this DVR value and the BP. Also, the ratios that appear in the formula, and the regression line (called yyf), which will allow visualizing the Logan plot.

The `dvr_values` function uses the `logan_niftypad` function to give the DVR and Logan plots for each subject and region.

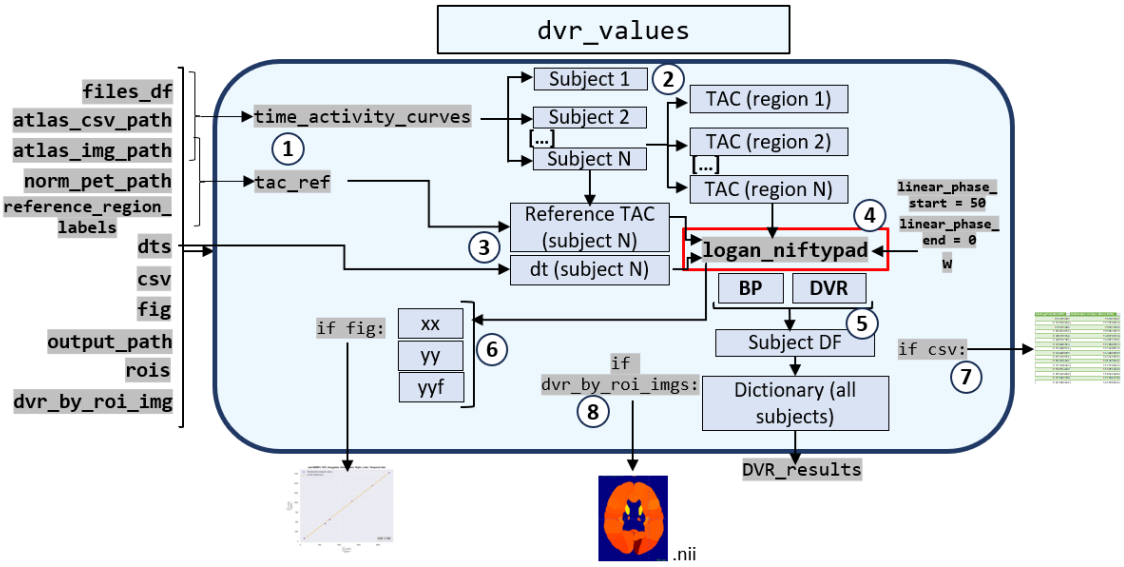

Figure 25. Diagram of the *dvr_values* function.

1	Use the `time_activity_curves` and `tac_ref` functions from the previous script.
2	For each subject, get the TAC of each specified ROI in the input `rois`.
3	Get the input function (from `tac_ref`) and time vector (from `dts`) of each subject.
4	Apply the `logan_niftypad` function to all subjects and ROIs. Linear phase start: 50. Linear phase end: 0. Weights: the same for all time frames.
5	Get the BP and DVR from the `logan_niftypad` outputs, and append them to a DataFrame for each subject, which will go in a dictionary with all subjects.
6	If `fig` is stated True, with the rest of the outputs from `logan_niftypad` we generate the Logan plot for each ROI and subject, and save them in `ouput_path`.
7	If `csv` is stated True, save each subject's DataFrame as a CSV file in `output_path`.
8	If `dvr_by_roi_imgs` is stated True, call the function `dvr_by_roi_img` and save the generated images in `output_path`.

Returns	`DVR_results`	*Dictionary.* Contains a DataFrame for each subject. Each DataFrame contains the BP and DVR for each ROI.

Table 8. Step-by-step explanation of the *dvr_values* function.

Figure 26 shows some examples of Logan plots generated by this function in different regions of the same subject. We can see how the linearity of Logan is achieved, which is considerably easy with our dataset since we only have six points.

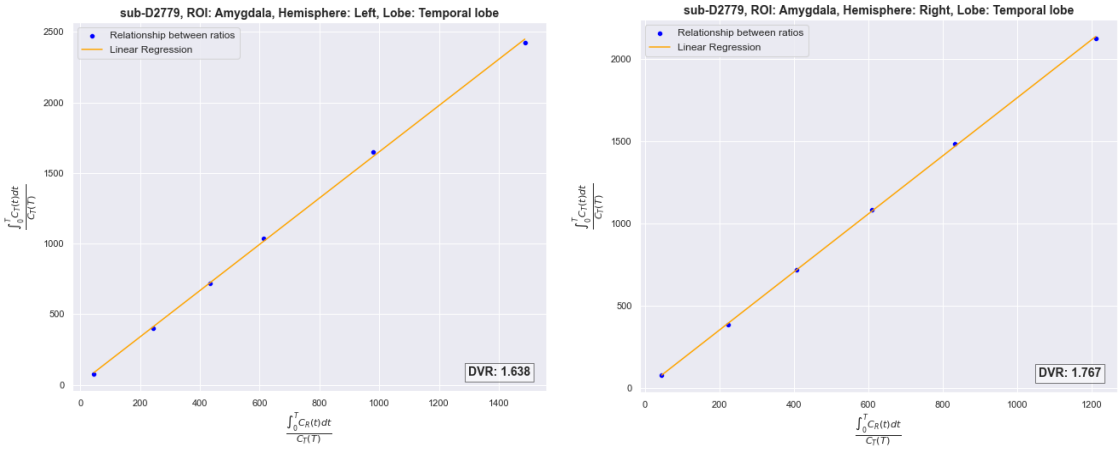

Figure 26. Logan plots of the amygdala (left and right) generated by the *dvr_values* function (subject D2779).

Figure 27 shows part of a CSV file from created by this function, where we can check the BP and DVR of a particular subject for each ROI.

ROI_NUM	ROI_NAME	ROI_HEMIS	ROI_LOBE	BP	DVR
1	Hippocampus	Left	Temporal lobe	0,6016	1,6016
2	Hippocampus	Right	Temporal lobe	0,5744	1,5744
3	Amygdala	Left	Temporal lobe	1,0765	2,0765
4	Amygdala	Right	Temporal lobe	1,1081	2,1081
5	Anterior temporal lobe medial part	Left	Temporal lobe	0,3777	1,3777
6	Anterior temporal lobe medial part	Right	Temporal lobe	0,4359	1,4359
7	Anterior temporal lobe lateral part	Left	Temporal lobe	0,1297	1,1297
8	Anterior temporal lobe lateral part	Right	Temporal lobe	0,1559	1,1559
9	Parahippocampal gyrus	Left	Temporal lobe	0,6283	1,6283
10	Parahippocampal gyrus	Right	Temporal lobe	0,6693	1,6693
11	Temporal superior posterior part	Left	Temporal lobe	0,0736	1,0736
12	Temporal superior posterior part	Right	Temporal lobe	0,1003	1,1003
13	Middle and inferior temporal gyrus	Left	Temporal lobe	0,1534	1,1534
14	Middle and inferior temporal gyrus	Right	Temporal lobe	0,1745	1,1745
15	Fusiform gyrus	Left	Temporal lobe	0,2281	1,2281
16	Fusiform gyrus	Right	Temporal lobe	0,4036	1,4036

Figure 27. CSV file created by the *dvr_values* function, showing the BP and DVR of the first 16 regions (subject D3553).

Same as with the SUVR, we can create NIfTI images for each subject where each ROI has its DVR as the intensity. This is done through the function **`dvr_by_roi_img`**, which works basically as the `suvr_by_roi_img` but using the DVR values instead of the SUVR, giving out images like the ones seen in Figure 20.

❖ DVR parametric images

Finally, we have a function that creates parametric images of the DVR for each subject, called **`parametric_img_dvr`**, where each voxel in the brain image will have an intensity of the DVR at that point. This works the same way as the `parametric_img_suvr`, but instead of normalizing each voxel by the reference region, we make them go through the `logan_niftypad` function. This function is put in a separate script because it takes quite a long (around 25 min per image), and couldn't find a way to optimize it.

Figure 28 shows three different parametric images of one subject from each group. In the control and aDS, there doesn't appear much difference, but there is a clear larger radiotracer uptake in the dDS subject, similarly to what we have previously seen with the SUVR parametric images.

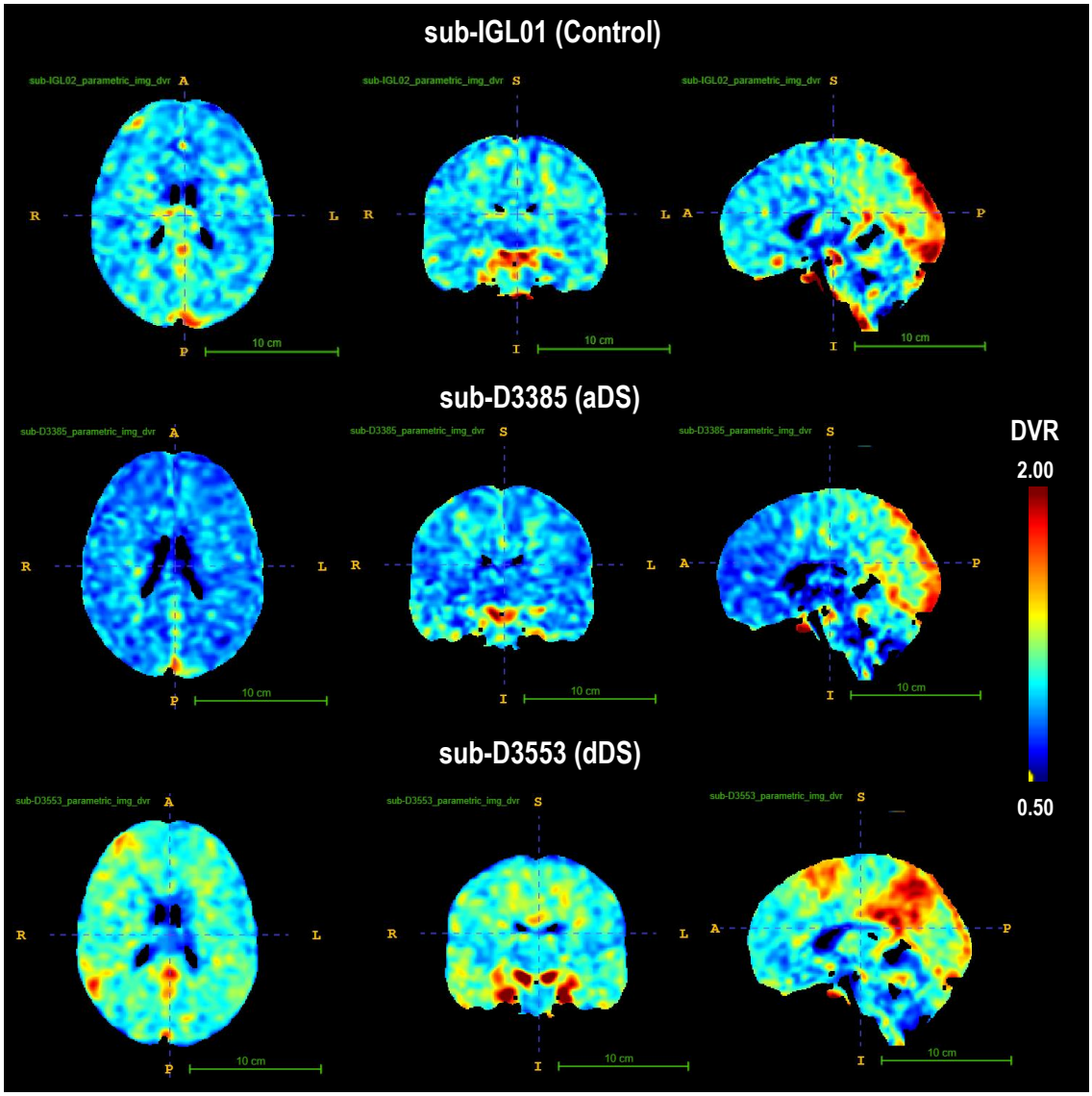

Figure 28. Axial, coronal and sagittal views of three DVR parametric images, and the corresponding colour scale. Each image corresponds to a subject from one of the three groups. Same as with the SUVR parametric images, we see a greater radiotracer uptake in the demented subject.

5.5 Analysis of the results and discussion

The final part of our code is aimed at analysing the results from our dataset and visualize them in different ways to evaluate if the software works as expected. We must compare the SUVR and DVR values between control, aDS and dDS subjects, to see which of them has an overall higher radiotracer uptake. We will compare different regions of the brain as well, to see which ones are more specific to the radiotracer.

To visualize the radiotracer uptake in the different ROIs in each subject group, Figure 29 shows slices from parametric images which have been created by averaging the parametric images in each group (made in a script named *mean_parametric_imgs*) and selecting specific ROIs.

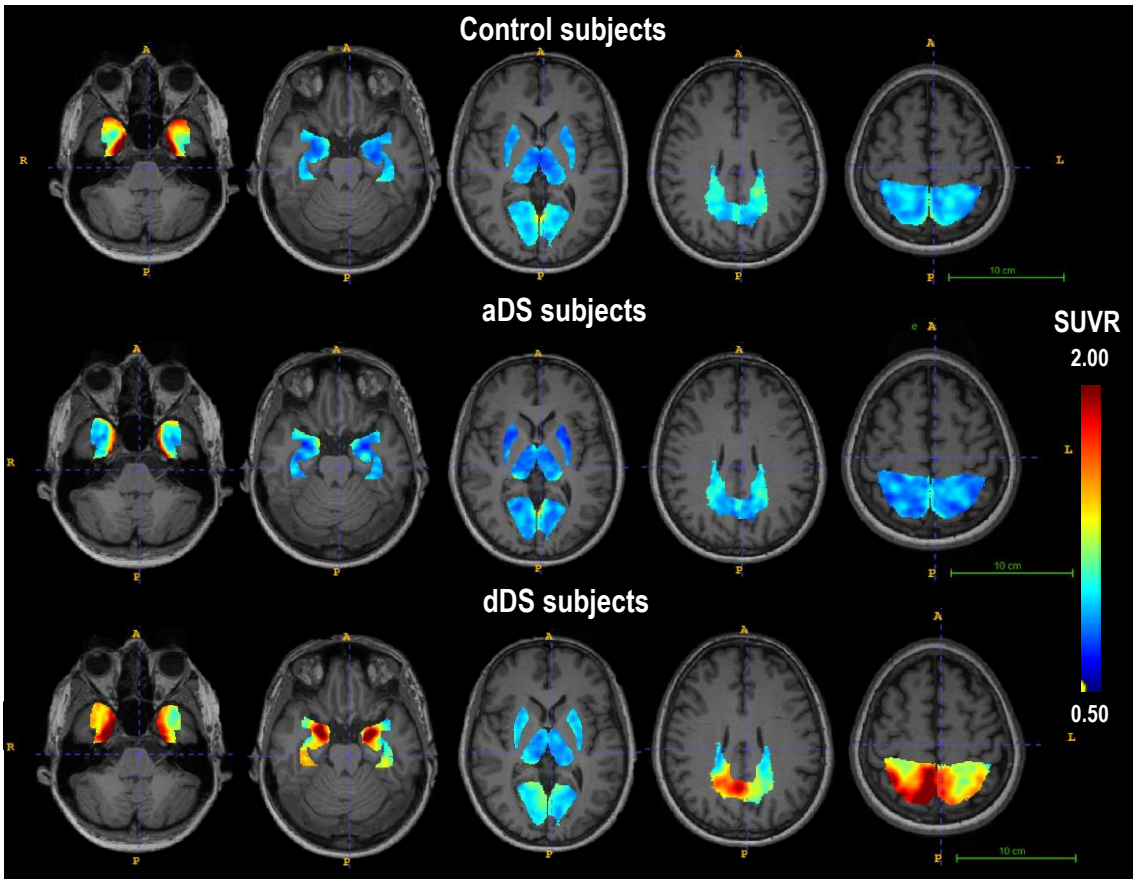

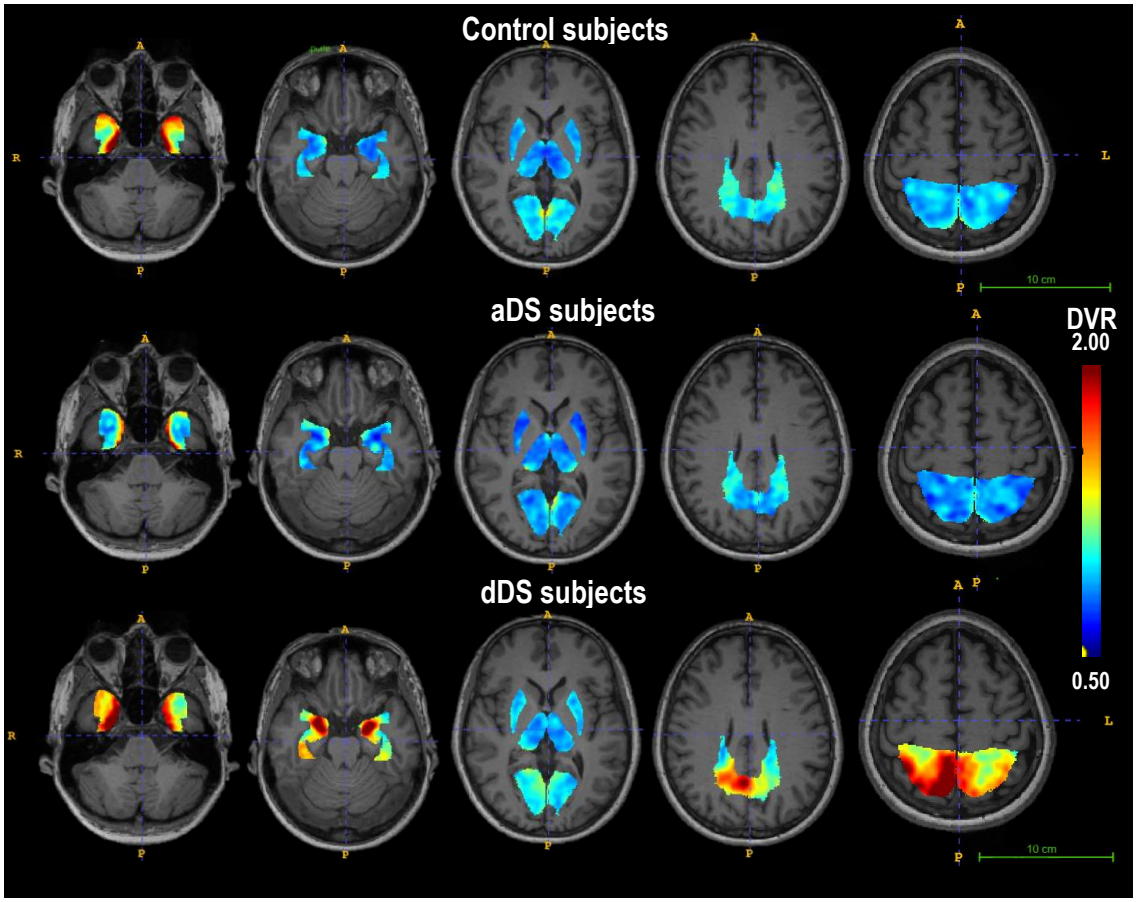

Figure 29. *SUVR and DVR average parametric images for the selected ROIs across subject types (axial view).*

Visually, clearly the radiotracer uptake is higher in dDS subjects, which makes sense considering these subjects have developed dementia, so the amount of tau aggregates should be higher as well. However, we can't appreciate much of a difference between control and aDS subjects. It is also noticeable that images showing the DVR are vastly similar from those showing the SUVR.

Taking into account the previous studies of 18F-PI-2620, and the regions we have available in our atlas, the ROIs we selected for this analysis are the amygdala (AG), anterior temporal lobe medial part (ATLMP), fusiform gyrus (FG), hippocampus (HC), lingual gyrus (LG), precuneus (PC), putamen (PT), and thalamus (TH), all of them for both the left and right hemispheres.

In a final script named *result_analysis*, we use the CSV files with the SUVR and DVR to visualize these results in different ways.

Figure 30 shows scatter plots for the SUVR and DVR values in the selected ROIs, in the left and right hemispheres. Each marker corresponds to a subject, while the shape and colour indicate the subject group.

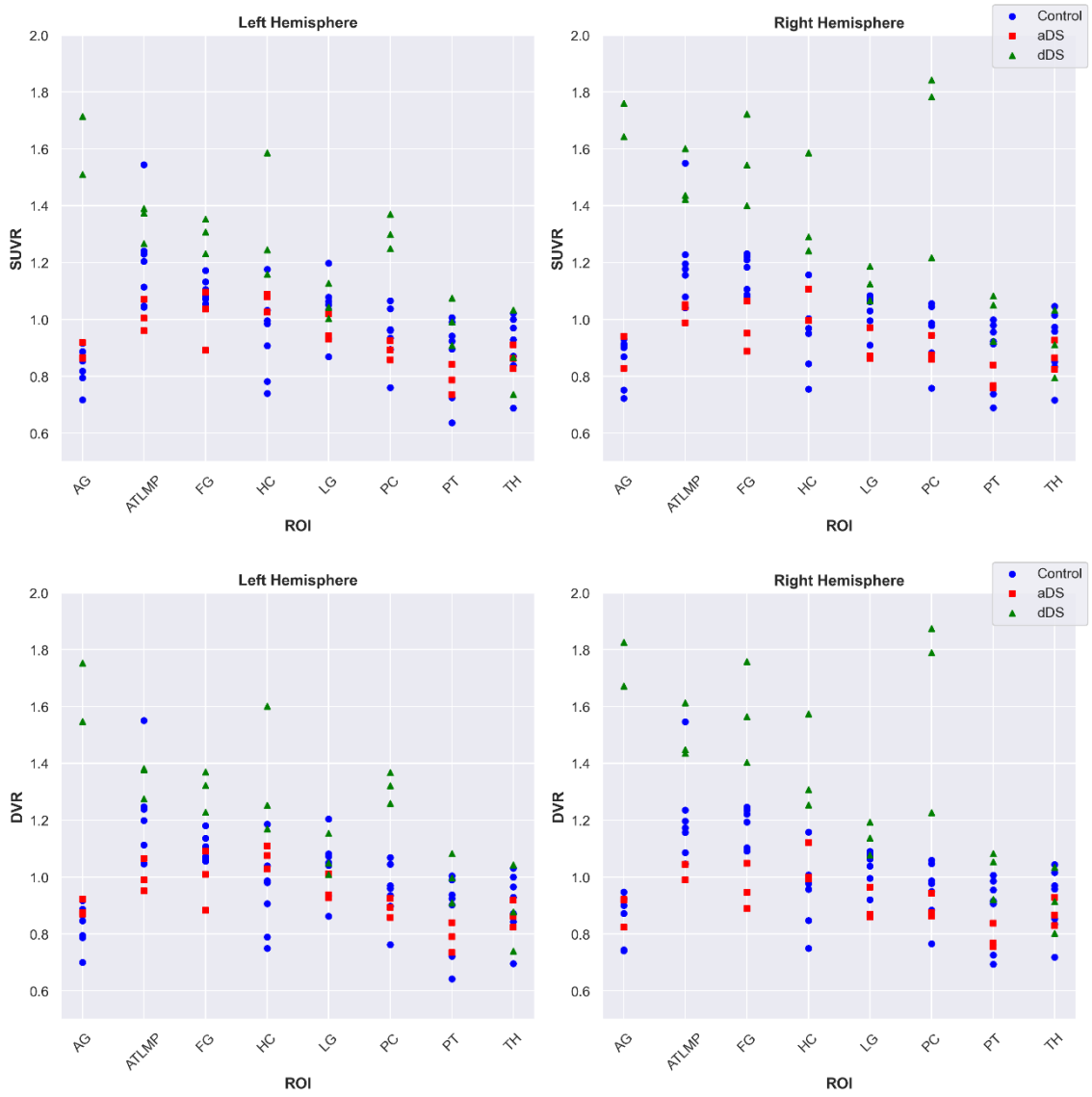

Figure 30. Scatter plots for the SUVR and DVR values in different ROIs (left and right hemispheres).

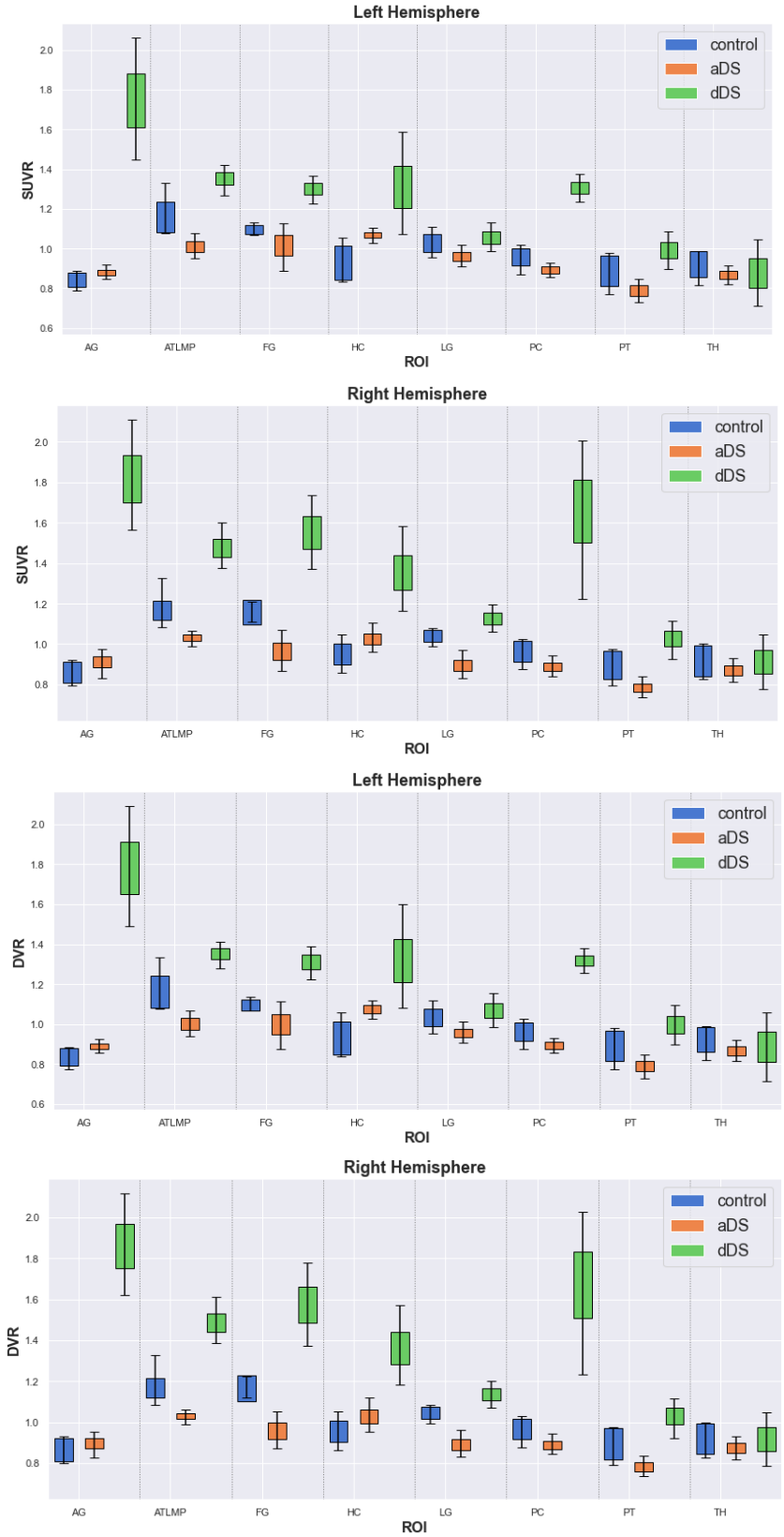

Figure 31. Boxplots of each subject group in each ROI.

Figure 31 displays boxplots with the mean SUVR/DVR values and their confidence intervals, for each ROI and each subject type (by averaging all subjects in each group), in both brain hemispheres. The confidence intervals around each box indicate the uncertainty or variability

around the mean and represents the range within the true population mean of the parameter is likely to fall, with a 95% level of confidence.

The results reveal significant 18F-PI-2620 binding differences among groups. Subjects with DS that have developed Alzheimer's (dDS) show significantly higher mean SUVR and DVR values overall. This group reveals an especially elevated radiotracer uptake in the amygdala and precuneus compared to the other subject groups. There is also a significant difference in the hippocampus, ATLMP and fusiform gyrus. This group also shows the highest variability, but their values are always considerably higher than in the other groups.

On the other hand, healthy controls and asymptomatic subjects don't show significant differences between them, nor between ROIs, so we can assume that subjects with DS that haven't developed dementia don't have an abnormal amount of tau aggregates. Additionally, the lingual gyrus, putamen and thalamus don't seem to be binding sites of the radiotracer, since the uptake is similar in the three groups.

These results indicate a good reliability of the radiotracer for the detection of AD, and most likely other tauopathies, which would include PSP. Moreover, the elevated affinity in regions such as the amygdala and precuneus could represent early markers of the pathology for this specific database.

The plots also suggest that the SUVR and DVR values are very similar, which highlights the data consistency, and seemingly dismisses the need to do a dynamic approach. However, this similarity is most likely due to the limited number of time frames we have, since the data set used in the analysis wasn't acquired for a strictly dynamic analysis, therefore the limitation in their acquired frames. We can't completely validate this relationship before conducting more consistent studies.

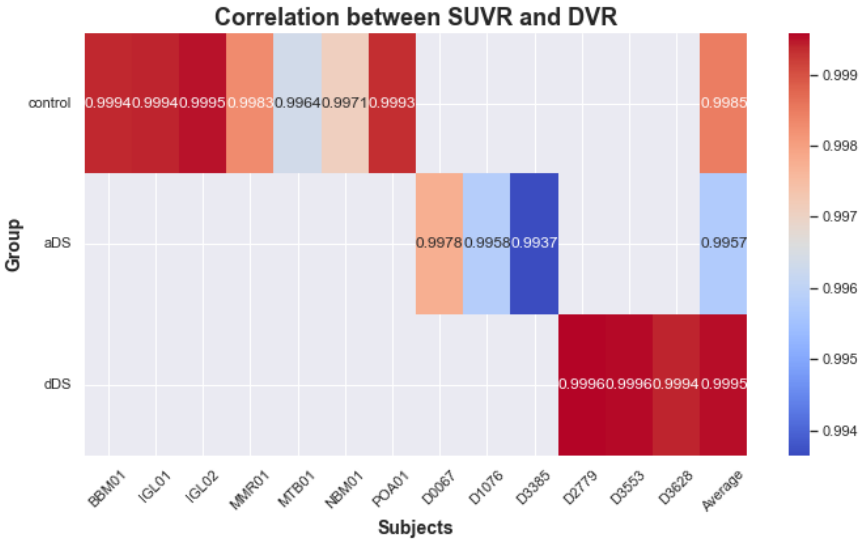

Figure 32. SUVR and DVR correlation heatmap for each subject and the average correlation of each subject group.

Figure 32 shows a heatmap with the correlation between SUVR and DVR values across shared ROIs for each subject. The results indicate a linear relationship between the two parameters. A large number of decimals is used to check if the SUVR and DVR were actually different, and turns out they are, although it is almost imperceptible. The colours in the heatmap can be misleading,

but seeing that the lowest value is 0.994, it means that the linear relationship is true for all subjects. These results show that the developed method for dynamic quantification is compatible with the static measurements in this set, confirming the availability of using the developed procedure with more specific dynamic acquisitions.

The result of this project is the developed software for quantification, which was the main proposed goal. After testing it with the provided image dataset and analysing the results, we see how the radiotracer behaves as expected, so we can confirm that the software works correctly, and can expect it to be useful for quantification of dynamic PET images in the future and detection of tauopathies such as PSP, more specifically with the 18F-PI-2620 radiotracer.

6. Workplan

This project has involved several tasks, from planning to the writing of this report. Figure 33 shows the work breakdown structure (WBS) of the project, where each task is organized in different sections.

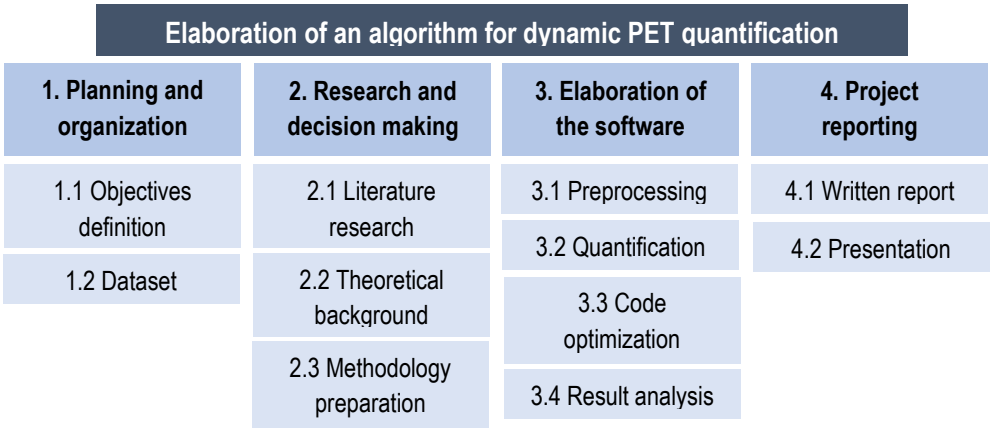

Figure 33. WBS of the project.

1. Planning and organization

N	Name	Duration	Description
1.1	Objectives definition	2 days	Understanding of the main goal of the project, definition of the scope and planification of the tasks.
1.2	Dataset obtention	5 days	Obtain the images used for the dataset and learn how to visualize and manipulate them.

2. Research and decision making

N	Name	Duration	Description
2.1	Literature research	15 days	Compile articles about previous studies made with 18F-PI-2620 to see the different methodology we can use for the quantification of PET images with this radiotracer.
2.2	Theoretical background	20 days	Do extensive research of the concepts surrounding dynamic PET imaging, kinetic modelling, and the different techniques for quantification of dynamic images.

2.3	Methodology preparation	10 days	Investigate and make the appropriate choices for the methodology we are going to use for the development of our software (parameters to quantify, the required image preprocessing, existing software we can use…) and obtain the necessary 'ingredients' for the elaboration of the code (templates, atlases, Python libraries…).

3. Elaboration of the software

N	Name	Duration	Description
3.1	Preprocessing	15 days	Start the software by programming the necessary preprocessing to the images, which include the coregistering of the PET images to anatomical images and template for segmentation.
3.2	Quantification	30 days	Write the code to perform the quantification with the chosen methods.
3.3	Code optimization	7 days	Review the complete code, organizing it in a unified and generalized manner, optimize the processes and review thoroughly the presence of any errors.
3.4	Result analysis	10 days	Test the software and write an additional code to make an appropriate analysis of the results obtained.

4. Project reporting

N	Name	Duration	Description
4.1	Written report	20 days	Write and deliver the report describing the project.
4.2	Presentation	7 days	Prepare and present an oral presentation about the project.

Table 9. Description of the tasks for the project.

The project is divided into four parts, with the third part (elaboration of the software) being the core of the work. Each part is composed of different tasks that must be accomplished in a certain order for the correct development of the project. These tasks take place during the first semester of the year 2023-24 (around 120 days), with an expected duration of 300 total hours. Table 9 has the detailed description of each task.

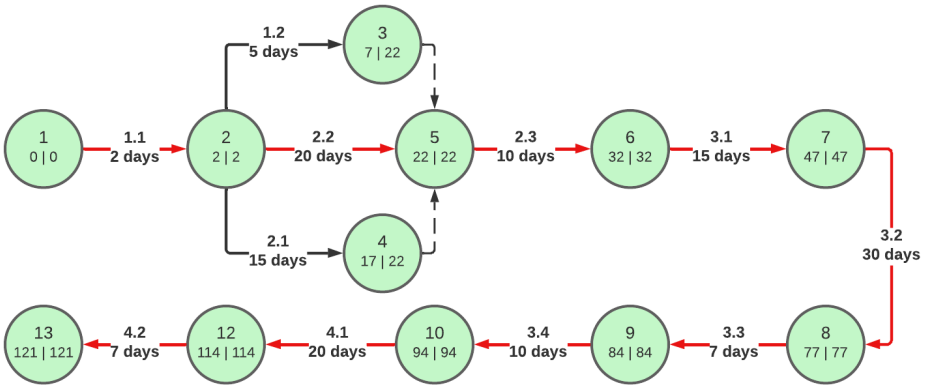

Figure 34. PERT diagram of the project. The critical path is in red.

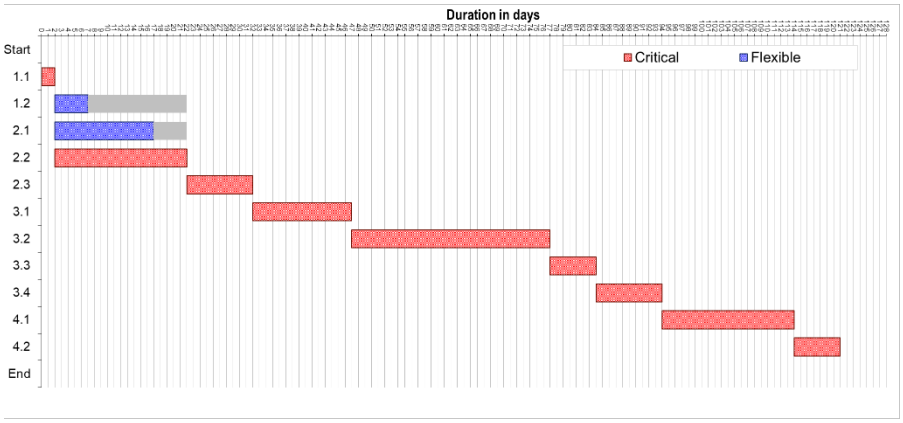

Figure 35. GANTT diagram of the project.

With the Program Evaluation and Review Technique (PERT) and the GANTT diagram, we can visualize the time distribution of the project in an ordered manner. For each task, we can see their precedent and posterior task to accomplish. The estimated time of the project is 121 days.

7. Technical viability

For the technical viability, we can use a SWOT analysis. This method incorporates an external and internal analysis that allows identification of the strengths, weaknesses, opportunities, and threats of our project.

Internal	External
Strengths	Opportunities
• Python programming • Local computers in the lab • BIG-UB help	• Useful tool for neurology • 18F-PI-2620 previous studies • Open-source software
Weaknesses	Threats
• Lack of experience in image processing and extensive coding. • Small dataset	• Unexpected technical difficulties • Limited time

Table 10. SWOT analysis of the project.

❖ **Strengths**

Python is completely free and allows performing so many tasks involving image processing, being one of the most used programming languages in this field, so a previous familiarity with this tool will help a lot. Moreover, the local computers in the biophysics lab will allow the code to run faster.

Also, the BIG-UB is very familiar with brain image processing in Python, which makes them very useful to ask for advice and solve issues during the development of the software.

❖ **Weaknesses**

Personally, I lack experience on image processing and have a low knowledge of kinetic modelling and dynamic image quantification, so for this project I must do a wide theoretical review. Also, although being familiar with Python, I have never made a code that involves so many tasks, so I must learn a lot about programming as well.

In addition, obtaining accurate and reliable data may be challenging due to the limited dataset we have, with just 13 subjects. The limited number of time frames in the dynamic acquisition might pose a problem as well.

❖ **Opportunities**

This project provides a tool for the quantification of dynamic PET images, very useful for neurological studies of rare diseases such as PSP and other tauopathies.

Since there are already several studies with the radiotracer 18F-PI-2620, we can use them to decide which methodology is the best to quantify in this type of studies, especially for dynamic quantification. Also, the existence of open-source software and Python libraries for image processing is something we can take advantage of.

❖ **Threats**

Software coding always involves unexpected technical or logistical challenges that can delay the progress or force us to dismiss some of the ideas for the project.

On the other hand, I must consider the limited time and the work I have outside of this project to be able to finish the project properly and in time.

8. Economic viability

The dataset we are using comes from 13 PET images acquired with the radiotracer 18F-PI-2620. Each radiotracer dose is around 1.200€. For the equipment and supplies used for developing the software we will add 4.000€ (computers, electricity…). The software development doesn't have any additional costs, but a theoretical amount for the 300 hours of work for this project could be around 20€/hour, adding up to 6.000€.

Concept/Item	Amount
Consumables (13 18F-PI-2620 doses)	15.600€
Equipment and supplies	4.000 €
Labour of software development	6.000 €
TOTAL	**23.000€**

Table 11. Estimated costs of the project.

9. Legal aspects

There are several legal aspects to consider in this project. First, the clinical trial to obtain the images has been performed according to *Real Decreto 1090/2015, de 4 de diciembre, por el que se regulan los ensayos clínicos con medicamentos, los Comités de Ética de la Investigación con medicamentos y el Registro Español de Estudios Clínicos* [70], which applies to all clinical trials with medicines of human use in Spain, including radiopharmaceuticals. The information about the 13 subjects whose images we have used is protected by the *Ley Orgánica 15/1999, de 13 de diciembre, de Protección de Datos de Carácter Personal* [71], and all the ethical guidelines have been followed, including informed consent from the participants, and responsible use of their data.

Also, I must mention that in Spain the radiotracer 18F-PI-2620 is currently used for AD studies, and still not approved for PSP. However, this project presents a methodology that can be used when PSP studies are allowed.

The software presented in this project is subject to title VII from *Real Decreto Legislativo 1/1996, de 12 de abril, por el que se aprueba el texto refundido de la Ley de Propiedad Intelectual, regularizando, aclarando y armonizando las disposiciones legales vigentes sobre la materia* [72]. This section states the protection of computer programs, which is considered an intellectual creation, whose rights are property of the UB Biomedical Imaging Group.

Regarding NiftyPAD and the function we have retrieved from it, the license states that we can use and modify their work, provided that we mention the original work and the changes [73]. The other Python libraries we have used are very common, and free to use for all users.

10. Conclusions and future improvements

As the life expectancy increases, the incidence of neurological disorders tends to increase as well. The early diagnosis of these diseases is crucial for the search of effective treatment, but is also challenging in some cases. Nonetheless, the advances in medical technology offer new ways for early diagnosis. PSP is one example of a neurodegenerative disease which currently can't be detected in-vivo, and its symptoms overlap with other parkinsonisms, making it more difficult to detect it in time. This project has presented a tau-specific PET tracer that has the potential revolutionize early detection of tauopathies such as PSP, known as 18F-PI-2620, by designing a quantification methodology and testing it with PET images acquired with said radiotracer.

The result of this project is the software for quantification which has been developed during these months. It includes two different approaches for quantification, selected due to their relevancy in previous studies with the radiotracer, those being the SUVR and DVR. The latter is the preferred approach, due to its ability to quantify dynamic images. SUVR is aimed at static acquisitions (using averaged images from the dynamic acquisition), but it has been very useful to evaluate the software method by comparing both methods. The dataset of images that was given for this project has allowed to test the developed software and given out results that confirm its correct functionality.

The comparison between the three groups from the dataset shows in which cases this radiotracer presents greater binding to the different regions of the brain. The radiotracer has shown a higher

uptake in subjects that have developed Alzheimer's, especially in regions such as the amygdala and the precuneus, which was the expected behaviour, so this validates the presented software. The potential for the radiotracer to identify tau aggregates and the affinity observed in specific brain regions offers a promising future for the diagnosis of tauopathies.

Both SUVR and Logan methods have shown very similar results, further confirming the correct functionality of the software. However, the images from the dataset used for the testing have a low number of time frames. This limitation hasn't allowed to test the software in dynamic images acquired with different conditions. Since the SUVR method is not really suited for dynamic studies, it is probable that it wouldn't be an accurate approach in studies with a larger amount of time frames. Also, it is possible that the Logan method wouldn't reach linearity as easily, so further testing is needed to confirm these hypotheses.

On the other hand, although our quantification methodology has shown to work properly, there are still improvements which can be implemented in the future. For instance, it would be possible improve the quality of the image during our image preprocessing, using methods such as partial volume correction, but this is left for a future version, due to our time limitations.

Another possible future improvement is the implementation of more models. Although the Logan graphical method seemed the most appropriate for this particular case, exploring a wider spectrum of quantification models would allow not only improving the precision of our results, but also expand the possibilities of application for this methodology to other medical conditions and PET tracers.

The development of a graphical interface for the software could be a great addition. Right now, it can be used by writing the necessary inputs into the code, but an intuitive interphase would allow users to do the process faster and more efficiently. Time limitations didn't allow this implementation, but it is something to consider if this software keeps evolving.

In conclusion, the developed software is a useful method for the quantification of dynamic PET images, which can be further improved in the future, and allows the evaluation of 18F-PI-2620 as an in-vivo diagnosis tool for tauopathies like PSP, when clinical trials for this disease start. It provides physiologically meaningful parameters, that are SUVR and DVR, that allow comparing the radiotracer uptake in the different regions of the brain, by knowing the mean value in each region, as well as visualizing them in parametric images. The combination of a solid methodology with continuous improvements and studies with different approaches will allow to keep moving forward towards more precise diagnosis and more effective treatment opportunities in the neurological field.

11. References

[1] "2018 Alzheimer's disease facts and figures," *Alzheimer's & Dementia*, vol. 14, no. 3, pp. 367–429, Mar. 2018, doi: 10.1016/J.JALZ.2018.02.001.

[2] T. Arendt, J. T. Stieler, and M. Holzer, "Tau and tauopathies," *Brain Res Bull*, vol. 126, pp. 238–292, Sep. 2016, doi: 10.1016/J.BRAINRESBULL.2016.08.018.

[3] L. Beyer and M. Brendel, "Imaging of Tau Pathology in Neurodegenerative Diseases: An Update," *Semin Nucl Med*, vol. 51, no. 3, pp. 253–263, May 2021, doi: 10.1053/J.SEMNUCLMED.2020.12.004.

[4] J. Levin, A. Kurz, T. Arzberger, A. Giese, and G. U. Höglinger, "The Differential Diagnosis and Treatment of Atypical Parkinsonism," *Dtsch Arztebl Int*, vol. 113, no. 5, pp. 61–69, Feb. 2016, doi: 10.3238/ARZTEBL.2016.0061.

[5] E. B. Mukaetova-Ladinska, C. R. Harrington, M. Roth, and C. M. Wischik, "Biochemical and anatomical redistribution of tau protein in Alzheimer's disease.," *Am J Pathol*, vol. 143, no. 2, p. 565, 1993, Accessed: Dec. 16, 2023. [Online]. Available: /pmc/articles/PMC1887045/?report=abstract

[6] M. Brendel *et al.*, "Assessment of 18F-PI-2620 as a Biomarker in Progressive Supranuclear Palsy," *JAMA Neurol*, vol. 77, no. 11, pp. 1408–1419, Nov. 2020, doi: 10.1001/JAMANEUROL.2020.2526.

[7] P. Alster, N. Madetko, D. Koziorowski, and A. Friedman, "Progressive Supranuclear Palsy-Parkinsonism Predominant (PSP-P)-A Clinical Challenge at the Boundaries of PSP and Parkinson's Disease (PD)," *Front Neurol*, vol. 11, Mar. 2020, doi: 10.3389/FNEUR.2020.00180.

[8] "Progressive supranuclear palsy - Symptoms and causes - Mayo Clinic." Accessed: Dec. 16, 2023. [Online]. Available: https://www.mayoclinic.org/diseases-conditions/progressive-supranuclear-palsy/symptoms-causes/syc-20355659

[9] H. Kroth *et al.*, "Discovery and preclinical characterization of [18F]PI-2620, a next-generation tau PET tracer for the assessment of tau pathology in Alzheimer's disease and other tauopathies," *Eur J Nucl Med Mol Imaging*, vol. 46, no. 10, pp. 2178–2189, Sep. 2019, doi: 10.1007/S00259-019-04397-2.

[10] P. A. Yushkevich *et al.*, "User-guided 3D active contour segmentation of anatomical structures: significantly improved efficiency and reliability," *Neuroimage*, vol. 31, no. 3, pp. 1116–1128, Jul. 2006, doi: 10.1016/J.NEUROIMAGE.2006.01.015.

[11] "[18F]PI2620 tau deposition increases along the Alzheimer's disease continuum in Down Syndrome and in presence of amyloid." Accessed: Dec. 16, 2023. [Online]. Available: https://alz.confex.com/alz/2023/meetingapp.cgi/Paper/79926

[12] "PET Scan: What It Is, Types, Purpose, Procedure & Results." Accessed: Dec. 16, 2023. [Online]. Available: https://my.clevelandclinic.org/health/diagnostics/10123-pet-scan

[13] "Positron Emission Tomography (PET) | Johns Hopkins Medicine." Accessed: Dec. 16, 2023. [Online]. Available: https://www.hopkinsmedicine.org/health/treatment-tests-and-therapies/positron-emission-tomography-pet

[14] A. Berger, "How Does It Work?: Positron emission tomography," *BMJ : British Medical Journal*, vol. 326, no. 7404, p. 1449, Jun. 2003, doi: 10.1136/BMJ.326.7404.1449.

[15] T. Jones and D. Townsend, "History and future technical innovation in positron emission tomography," *J Med Imaging (Bellingham)*, vol. 4, no. 1, p. 011013, Mar. 2017, doi: 10.1117/1.JMI.4.1.011013.

[16] G. Wang, "High Temporal-Resolution Dynamic PET Image Reconstruction Using a New Spatiotemporal Kernel Method," *IEEE Trans Med Imaging*, vol. 38, no. 3, p. 664, Mar. 2019, doi: 10.1109/TMI.2018.2869868.

[17] G. Wang, A. Rahmim, and R. N. Gunn, "PET Parametric Imaging: Past, Present, and Future," *IEEE Trans Radiat Plasma Med Sci*, vol. 4, no. 6, p. 663, Nov. 2020, doi: 10.1109/TRPMS.2020.3025086.

[18] J. M. M. Rogasch, F. Hofheinz, L. van Heek, C. A. Voltin, R. Boellaard, and C. Kobe, "Influences on PET Quantification and Interpretation," *Diagnostics*, vol. 12, no. 2, Feb. 2022, doi: 10.3390/DIAGNOSTICS12020451.

[19] R. Sekerak, "Voxel," *Encyclopedia of Clinical Neuropsychology*, pp. 2662–2663, 2011, doi: 10.1007/978-0-387-79948-3_82.

[20] "TPC - PET data." Accessed: Dec. 16, 2023. [Online]. Available: http://www.turkupetcentre.net/petanalysis/pet_data.html

[21] J. M. M. Rogasch, F. Hofheinz, L. van Heek, C. A. Voltin, R. Boellaard, and C. Kobe, "Influences on PET Quantification and Interpretation," *Diagnostics (Basel)*, vol. 12, no. 2, Feb. 2022, doi: 10.3390/DIAGNOSTICS12020451.

[22] "Magnetism - Questions and Answers in MRI." Accessed: Dec. 16, 2023. [Online]. Available: https://mriquestions.com/registrationnormalization.html

[23] "ySMIN | young Spanish Molecular Imaging Network – e-smi.eu." Accessed: Dec. 16, 2023. [Online]. Available: https://e-smi.eu/young-esmi/yesmi-groups/ysmin/

[24] "TPC - Input function." Accessed: Dec. 16, 2023. [Online]. Available: http://www.turkupetcentre.net/petanalysis/input_function.html

[25] "Introduction To Kinetic Modeling (Part 1) [L39] - YouTube." Accessed: Dec. 16, 2023. [Online]. Available: https://www.youtube.com/watch?v=W2_OZYsAOoA&t=2s

[26] "TPC - Compartmental models in positron emission tomography." Accessed: Dec. 16, 2023. [Online]. Available: http://www.turkupetcentre.net/petanalysis/model_compartmental.html

[27] N. Holford and D. S. Yim, "Volume of Distribution," *Transl Clin Pharmacol*, vol. 24, no. 2, pp. 74–77, Jul. 2023, doi: 10.12793/tcp.2016.24.2.74.

[28] "TPC - Spectral analysis." Accessed: Dec. 16, 2023. [Online]. Available: http://www.turkupetcentre.net/petanalysis/model_spectral_analysis.html

[29] P. E. Kinahan and J. W. Fletcher, "Positron emission tomography-computed tomography standardized uptake values in clinical practice and assessing response to therapy," *Semin Ultrasound CT MR*, vol. 31, no. 6, pp. 496–505, Dec. 2010, doi: 10.1053/J.SULT.2010.10.001.

[30] "TPC - tissue-to-reference ratio." Accessed: Dec. 16, 2023. [Online]. Available: http://www.turkupetcentre.net/petanalysis/model_ref_ratio.html

[31] "TPC - MTGA." Accessed: Dec. 16, 2023. [Online]. Available: http://www.turkupetcentre.net/petanalysis/model_mtga.html

[32] "TPC - Reference input compartmental models." Accessed: Dec. 16, 2023. [Online]. Available: http://www.turkupetcentre.net/petanalysis/model_compartmental_ref.html

[33] M. Oh *et al.*, "Clinical Evaluation of 18F-PI-2620 as a Potent PET Radiotracer Imaging Tau Protein in Alzheimer Disease and Other Neurodegenerative Diseases Compared With 18F-THK-5351," *Clin Nucl Med*, vol. 45, no. 11, pp. 841–847, Nov. 2020, doi: 10.1097/RLU.0000000000003261.

[34] L. Beyer *et al.*, "Early-phase [18F]PI-2620 tau-PET imaging as a surrogate marker of neuronal injury," *Eur J Nucl Med Mol Imaging*, vol. 47, no. 12, pp. 2911–2922, Nov. 2020, doi: 10.1007/S00259-020-04788-W.

[35] S. Bullich *et al.*, "Evaluation of Dosimetry, Quantitative Methods, and Test-Retest Variability of 18F-PI-2620 PET for the Assessment of Tau Deposits in the Human Brain," *J Nucl Med*, vol. 61, no. 6, pp. 920–927, Jun. 2020, doi: 10.2967/JNUMED.119.236240.

[36] C. Chotipanich, M. Nivorn, A. Kunawudhi, C. Promteangtrong, N. Boonkawin, and A. Jantarato, "Evaluation of Imaging Windows for Tau PET Imaging Using 18F-PI2620 in Cognitively Normal Individuals, Mild Cognitive Impairment, and Alzheimer's Disease Patients," *Mol Imaging*, vol. 19, 2020, doi: 10.1177/1536012120947582.

[37] M. Song *et al.*, "Binding characteristics of [18F]PI-2620 distinguish the clinically predicted tau isoform in different tauopathies by PET," *J Cereb Blood Flow Metab*, vol. 41, no. 11, pp. 2957–2972, Nov. 2021, doi: 10.1177/0271678X211018904.

[38] T. Tezuka *et al.*, "Evaluation of [18F]PI-2620, a second-generation selective tau tracer, for assessing four-repeat tauopathies," *Brain Commun*, vol. 3, no. 4, 2021, doi: 10.1093/BRAINCOMMS/FCAB190.

[39] M. Song *et al.*, "Feasibility of short imaging protocols for [18F]PI-2620 tau-PET in progressive supranuclear palsy," *Eur J Nucl Med Mol Imaging*, vol. 48, no. 12, pp. 3872–3885, Nov. 2021, doi: 10.1007/S00259-021-05391-3.

[40] M. L. Carlson *et al.*, "Hippocampal subfield imaging and fractional anisotropy show parallel changes in Alzheimer's disease tau progression using simultaneous tau-PET/MRI at 3T," *Alzheimers Dement (Amst)*, vol. 13, no. 1, 2021, doi: 10.1002/DAD2.12218.

[41] S. Katzdobler *et al.*, "Additive value of [18F]PI-2620 perfusion imaging in progressive supranuclear palsy and corticobasal syndrome," *Eur J Nucl Med Mol Imaging*, vol. 50, no. 2, pp. 423–434, Jan. 2023, doi: 10.1007/S00259-022-05964-W.

[42] F. Völter *et al.*, "Assessment of perfusion deficit with early phases of [18F]PI-2620 tau-PET versus [18F]flutemetamol-amyloid-PET recordings," *Eur J Nucl Med Mol Imaging*, vol. 50, no. 5, p. 1384, Apr. 2023, doi: 10.1007/S00259-022-06087-Y.

[43] E. C. Mormino *et al.*, "Tau PET imaging with 18F-PI-2620 in aging and neurodegenerative diseases," *Eur J Nucl Med Mol Imaging*, vol. 48, no. 7, pp. 2233–2244, Jul. 2021, doi: 10.1007/S00259-020-04923-7.

[44] H. Kroth *et al.*, "PI-2620 Lead Optimization Highlights the Importance of Off-Target Assays to Develop a PET Tracer for the Detection of Pathological Aggregated Tau in Alzheimer's Disease and Other Tauopathies," *J Med Chem*, vol. 64, no. 17, pp. 12808–12830, Sep. 2021, doi: 10.1021/ACS.JMEDCHEM.1C00861.

[45] A. L. Boxer, J. T. Yu, L. I. Golbe, I. Litvan, A. E. Lang, and G. U. Höglinger, "Advances in progressive supranuclear palsy: new diagnostic criteria, biomarkers, and therapeutic approaches," *Lancet Neurol*, vol. 16, no. 7, pp. 552–563, Jul. 2017, doi: 10.1016/S1474-4422(17)30157-6.

[46] M. Brendel *et al.*, "[18F]-THK5351 PET Correlates with Topology and Symptom Severity in Progressive Supranuclear Palsy," *Front Aging Neurosci*, vol. 9, no. JAN, Jan. 2018, doi: 10.3389/FNAGI.2017.00440.

[47] "NMMItools – Tools for Nuclear Medicine and Molecular Imaging Research." Accessed: Dec. 16, 2023. [Online]. Available: https://nmmitools.org/

[48] J. Kang, Y. Gao, F. Shi, D. S. Lalush, W. Lin, and D. Shen, "Prediction of standard-dose brain PET image by using MRI and low-dose brain [18F]FDG PET images," *Med Phys*, vol. 42, no. 9, p. 5301, Sep. 2015, doi: 10.1118/1.4928400.

[49] L. Xiang *et al.*, "Deep Auto-context Convolutional Neural Networks for Standard-Dose PET Image Estimation from Low-Dose PET/MRI," *Neurocomputing*, vol. 267, pp. 406–416, Dec. 2017, doi: 10.1016/J.NEUCOM.2017.06.048.

[50] "Neuroimaging in Python — NiBabel 5.3.0.dev5+g773e3c40 documentation." Accessed: Dec. 17, 2023. [Online]. Available: https://nipy.org/nibabel/manual.html#manual

[51] "Atlases - FslWiki." Accessed: Jan. 21, 2024. [Online]. Available: https://fsl.fmrib.ox.ac.uk/fsl/fslwiki/Atlases

[52] "ANTsX/ANTsPy: Advanced Normalization Tools in Python." Accessed: Dec. 16, 2023. [Online]. Available: https://github.com/ANTsX/ANTsPy

[53] T. Zhang *et al.*, "Spatial normalization and quantification approaches of PET imaging for neurological disorders," *European Journal of Nuclear Medicine and Molecular Imaging 2022 49:11*, vol. 49, no. 11, pp. 3809–3829, May 2022, doi: 10.1007/S00259-022-05809-6.

[54] "Individual Adult Brain Atlases – Brain Development." Accessed: Jan. 22, 2024. [Online]. Available: https://brain-development.org/brain-atlases/adult-brain-atlases/individual-adult-brain-atlases/

[55] J. Yang *et al.*, "Partial volume correction for PET quantification and its impact on brain network in Alzheimer's disease," *Scientific Reports 2017 7:1*, vol. 7, no. 1, pp. 1–14, Oct. 2017, doi: 10.1038/s41598-017-13339-7.

[56] J. Logan, J. S. Fowler, N. D. Volkow, G. J. Wang, Y. S. Ding, and D. L. Alexoff, "Distribution volume ratios without blood sampling from graphical analysis of PET data," *J Cereb Blood Flow Metab*, vol. 16, no. 5, pp. 834–840, 1996, doi: 10.1097/00004647-199609000-00008.

[57] "TPC - Regional Logan plot - calculation with reference input." Accessed: Dec. 16, 2023. [Online]. Available: http://www.turkupetcentre.net/petanalysis/model_logan_ref.html

[58] T. Funck, K. Larcher, P. J. Toussaint, A. C. Evans, and A. Thiel, "APPIAN: Automated Pipeline for PET Image Analysis," *Front Neuroinform*, vol. 12, Sep. 2018, doi: 10.3389/FNINF.2018.00064.

[59] J. Jiao *et al.*, "NiftyPAD - Novel Python Package for Quantitative Analysis of Dynamic PET Data," *Neuroinformatics*, vol. 21, no. 2, pp. 457–468, Apr. 2023, doi: 10.1007/S12021-022-09616-0.

[60] "ANTsPy documentation — ANTsPy master documentation." Accessed: Dec. 17, 2023. [Online]. Available: https://antspy.readthedocs.io/en/latest/

[61] "json — JSON encoder and decoder — Python 3.12.1 documentation." Accessed: Dec. 17, 2023. [Online]. Available: https://docs.python.org/3/library/json.html

[62] "User guide: contents — scikit-learn 1.3.2 documentation." Accessed: Dec. 17, 2023. [Online]. Available: https://scikit-learn.org/stable/user_guide.html

[63] "User guide and tutorial — seaborn 0.13.0 documentation." Accessed: Dec. 17, 2023. [Online]. Available: https://seaborn.pydata.org/tutorial.html

[64] "matplotlib.pyplot — Matplotlib 3.8.2 documentation." Accessed: Dec. 17, 2023. [Online]. Available: https://matplotlib.org/stable/api/pyplot_summary.html

[65] "os — Miscellaneous operating system interfaces — Python 3.12.1 documentation." Accessed: Dec. 17, 2023. [Online]. Available: https://docs.python.org/3/library/os.html

[66] "AMYPAD/NiftyPAD: Neuroimaging for the Prevention of Alzheimer's Disease." Accessed: Dec. 17, 2023. [Online]. Available: https://github.com/AMYPAD/NiftyPAD

[67] "NumPy user guide — NumPy v1.26 Manual." Accessed: Dec. 17, 2023. [Online]. Available: https://numpy.org/doc/stable/user/index.html#user

[68] "SciPy User Guide — SciPy v1.11.4 Manual." Accessed: Dec. 17, 2023. [Online]. Available: https://docs.scipy.org/doc/scipy/tutorial/index.html#user-guide

[69] "User Guide — pandas 2.1.4 documentation." Accessed: Dec. 17, 2023. [Online]. Available: https://pandas.pydata.org/docs/user_guide/index.html

[70] "BOE-A-2015-14082 Real Decreto 1090/2015, de 4 de diciembre, por el que se regulan los ensayos clínicos con medicamentos, los Comités de Ética de la Investigación con medicamentos y el Registro Español de Estudios Clínicos." Accessed: Dec. 27, 2023. [Online]. Available: https://www.boe.es/diario_boe/txt.php?id=BOE-A-2015-14082

[71] "BOE-A-1999-23750 Ley Orgánica 15/1999, de 13 de diciembre, de Protección de Datos de Carácter Personal." Accessed: Dec. 27, 2023. [Online]. Available: https://www.boe.es/buscar/act.php?id=BOE-A-1999-23750

[72] "BOE-A-1996-8930 Real Decreto Legislativo 1/1996, de 12 de abril, por el que se aprueba el texto refundido de la Ley de Propiedad Intelectual, regularizando, aclarando y armonizando las disposiciones legales vigentes sobre la materia." Accessed: Dec. 27, 2023. [Online]. Available: https://www.boe.es/buscar/act.php?id=BOE-A-1996-8930

[73] "NiftyPAD/LICENSE at master · JJiao/NiftyPAD." Accessed: Dec. 27, 2023. [Online]. Available: https://github.com/JJiao/NiftyPAD/blob/master/LICENSE

[74] "[18F]PI-2620 | Chemical Substance Information | J-GLOBAL." Accessed: Dec. 16, 2023. [Online]. Available: https://jglobal.jst.go.jp/en/detail?JGLOBAL_ID=202007016307296642

[75] "Biograph Vision PET/CT Scanner - Siemens Healthineers USA." Accessed: Dec. 16, 2023. [Online]. Available: https://www.siemens-healthineers.com/en-us/molecular-imaging/pet-ct/biograph-vision

[76] G. J. Matheson, "kinfitr: Reproducible PET Pharmacokinetic Modelling in R," *bioRxiv*, p. 755751, Sep. 2019, doi: 10.1101/755751.

[77] D. N. Greve *et al.*, "Cortical surface-based analysis reduces bias and variance in kinetic modeling of brain PET data," *Neuroimage*, vol. 92, pp. 225–236, May 2014, doi: 10.1016/J.NEUROIMAGE.2013.12.021.

[78] "PMOD Technologies LLC – PMOD Technologies." Accessed: Dec. 16, 2023. [Online]. Available: https://www.pmod.com/web/

[79] T. Karjalainen *et al.*, "Magia: Robust Automated Image Processing and Kinetic Modeling Toolbox for PET Neuroinformatics," *Front Neuroinform*, vol. 14, Feb. 2020, doi: 10.3389/FNINF.2020.00003/FULL.

[80] "bilgelm/dynamicpet: Dynamic positron emission tomography (PET) analysis." Accessed: Dec. 16, 2023. [Online]. Available: https://github.com/bilgelm/dynamicpet

[81] F. J. López-González *et al.*, "QModeling: a Multiplatform, Easy-to-Use and Open-Source Toolbox for PET Kinetic Analysis," *Neuroinformatics*, vol. 17, no. 1, pp. 103–114, Jan. 2019, doi: 10.1007/S12021-018-9384-Y.

Annexes

❖ Tables describing previous 18F-PI-2620 studies:

Acquisition

Article	Goal of 18F-PI-2620	Acquisition/ injected dose	Acquisition time
Brendel M (2020) [6]	Biomarker in PSP	Dynamic 168 to 334 MBq	0-60 min and 80-120 min (5-minute frames)
Minyoung O (2020) [33]	Radiotracer compared with 18F-THK-5351 in AD	Static 259 ± 25.9 MBq	60-90 min post injection
Beyer L (2020) [34]	Surrogate marker of neuronal injury	Dynamic 185±10 MBq	0-60 min post injection
Bullich S (2020) [35]	Assessment of Tau Deposits in the Human Brain	Dynamic 339.4± 5.2 and 339.7±7.5 MBq	180 min (0–90 min: 6x30 s, 4x1min, 4x2 min, and 15x5 min; 120–180 min: 12x5min)
Chotipanich C (2020) [36]	Evaluation for CNI, MCI, and AD patients	Dynamic 185 MBq	0-45 min post injection
Song M (2021) [37]	Distinguish tau isoforms in different tauopathies	Dynamic 217±53 MBq	0-60 min, framed into 6x30s, 4x60s,4x120sand9x300s
Tezuka T (2021) [38]	Assessing four-repeat tauopathies	Static 185 MBq ± 10%	60-90 min post injection
Song M (2021) [39]	Imaging protocols in PSP	Dynamic 168 to 334 MBq	0-60 min post injection
Carlson M (2021) [40]	Parallel changes in Alzheimer's disease tau progression	Dynamic 5 to 10 mCi	0-90 min post injection
Kroth H (2021) [44]	Detection of pathological aggregated tau in AD and other Tauopathies	Dynamic 185 MBq	30-75 min post injection
Mormino E (2021) [43]	Imaging in aging and ND	Dynamic 5 to 10 mCi	60-90 min post injection
Völter F (2023) [42]	Comparation with [18F]flutemetamol-amyloid -PET recordings	Dynamic 151 to 223 MBq	0-60 min post injection
Katzdobler S (2023) [41]	Imaging in PSP and CBS	Dynamic 185±10 MBq	0-60 min post injection framed into 6x30 s, 4x60 s, 4x120 s, and 9x300 s

Table 12. Acquisition in different 18F-PI-2620 studies

Coregistration and segmentation

Article	Software or method used	Atlas	VOIs
Brendel M (2020) [6]	PMOD	Brainnetome atlas and Hammers atlas	Globus pallidus (internus and externus), Putamen, Subthalamic nucleus, Substantia nigra, Dorsal midbrain, Dentate nucleus, Dorsolateral prefrontal cortex, Medial prefrontal cortex.
Minyoung O (2020) [33]	FreeSurfer and manually	Deskian-Killiany atlas	Hippocampus, Amygdala, Striatum, Pallidum, Substantia nigra
Beyer L (2020) [34]	PMOD	Hammers atlas	Cortical volumes: Bilateral frontal, Central region, Parietal, Temporal, Occipital
Bullich S (2020) [35]	Template and normalized grey matter segmentation intersection	Automatic Anatomic Labelling template	Amygdala, Hippocampus, Parahippocampus, Fusiform gyrus, Prefrontal cortex, Occipital cortex, Parietal cortex, Anterior cingulate cortex, Posterior cingulate cortex
Chotipanich C (2020) [36]	VOIs automatically outlined based on maximum probability following the atlas.	Automatic Anatomic Labelling template	Hippocampus, Inferior temporal lobe, Lingual gyrus, Middle temporal lobe, Occipital lobe, Parahippocampus, Parietal lobe, Posterior cingulate gyrus, Praecuneus, Fusiform, White matter
Song M (2021) [37]	PMOD	Hammers atlas	Cortical volumes, Frontal, Occipital, Parietal, Temporal, Subcortical volumes, Putamen, Globus pallidus
Tezuka T (2021) [38]	PMOD and FreeSurfer	Probabilistic atlas in FreeSurfer	Caudate nucleus, Globus pallidus, Putamen, Thalamus, Superior frontal gyrus, Precentral gyrus, Midbrain, Pons
Song M (2021) [39]	PMOD	Hammers and ATAG atlases	Dorsolateral and medial prefrontal cortex, Internal and external part of the globus pallidus, Putamen, Subthalamic nucleus, Substantia nigra, Dorsal midbrain
Carlson M (2021) [40]	FreeSurfer	Custom atlas (combines multi-atlas label fusion and machine learning)	Dentate gyrus, Subiculum, Entorhinal and perinatal cortices, White matter

Kroth H (2021) [44]	PMOD	Automated anatomical labelling-merged atlas	Hippocampus, Fusiform gyrus, Middle temporal region, Parahippocampus region, Lingual region, Occipital region, Praecuneus region, Parietal region, Caudate region, Putamen, Thalamus
Mormino E (2021) [43]	FSL, FreeSurfer	FreeSurfer atlas	Medial temporal lobe, entorhinal, hippocampus, and amygdala, Posterior cingulate, Lateral parietal cortex
Völter F (2023) [42]	PMOD	Brainnetome atlas	246 regions of the Brainnetome atlas
Katzdobler S (2023) [41]	PMOD ANTs	Brainnetome atlas	246 regions of the Brainnetome atlas

Table 13. Coregistration and segmentation in different 18F-PI-2620 studies.

Quantification

Article	Software/method	Extracted parameters	Reference region
Brendel M (2020) [6]	PMOD	-DVR	Cerebellum
Minyoung O (2020) [33]	FreeSurfer	Mean SUVR	Inferior cerebellum
Beyer L (2020) [34]	PMOD	SUVR of different time frames	Cerebellum
Bullich S (2020) [35]	PMOD Compartmental models, and Logan graphical analysis	-Volume of distribution (VT) -DVR	Cerebellar cortex
Chotipanich C (2020) [36]	PMOD	SUVR of each frame	Cerebellum
Song M (2021) [37]	PMOD Logan graphical plots	-DVR -Average SUVR at different time points	Cerebellar grey matter

Tezuka T (2021) [38]	PMOD -Multilinear reference tissue model 2 (MRTM2) -Non-invasive kinetic modelling (SRTM, SRTM2 and MRTM2)	-DVR -SUVR for each frame	Dentate nucleus, central cerebellar white matter, superior and the posterior cerebellar layers
Song M (2021) [39]	FSL	SUVR	Cerebellar cortex and pericalcarine area
Carlson M (2021) [40]	PMOD (MRTM2)	-DVR -SUVR from static images (20–40, 30–50, and 40–60 min p.i.)	Superior and posterior cerebellar layers
Kroth H (2021) [44]	FreeSurfer	SUV from static images by summing the 30-minute interval between 60 and 90 minutes.	Inferior cerebellar cortex
Mormino E (2021) [43]	PMOD	SUVR	Cerebellum
Völter F (2023) [42]	FSL	SUVR of summed data corresponding to 60 to 90 min post-injection	Inferior cerebellum
Katzdobler S (2023) [41]	PMOD	SUVR	Cerebellum
Brendel M (2020) [6]	PMOD	SUVR	Cerebellum

Table 14. Quantification in different 18F-PI-2620 studies.